NTNU

Norwegian University of
Science and Technology

Acoustic communication for use in underwater sensor networks

Ole Trygve Haug

Master of Science in Electronics
Submission date: July 2009
Supervisor: Jens Martin Hovem, IET

Norwegian University of Science and Technology
Department of Electronics and Telecommunications

Problem Description

Design and simulation of an underwater acoustic communication system by using the EasyPLR program (PlaneRay), with focus on the modulation techniques. Evaluate the performance for different transmission distances with different levels of noise. Study different types of pulses and how varying the carrier frequency will affect the transmission loss.

Assignment given: 15. January 2009
Supervisor: Jens Martin Hovem, IET

Abstract

In this study an underwater acoustic communications system has been simulated. The simulations has been performed through use of a simulation program called EasyPLR that is based on the PlaneRay propagation model. In the simulations different pulse shapes have been tested for use in underwater communication. Different types of loss have also been studied for different carrier frequencies. Changing the carrier frequency from 20 kHz to 75 kHz gives a huge difference in both absorption loss and reflection loss. This means that there will be a tradeoff between having a high frequency for high data rate and reducing the carrier frequency to reduce the loss. The modulation technique used in this study is Quadrature phase shift keying and different sound speed profiles have been tested to see how this affects the performance. The transmission distance has been tested for several distances up to 3 km. The results show a significant difference in the performances at 1 km and 3 km for the same noise level. Direct sequence spread spectrum with Quadrature phase shift keying has also been simulated for different distances with good performance. The challenge is to get good time synchronization, and the performance is much better at 1 km than at 3 km.

Preface

This Master thesis has been written by Ole Trygve Haug on the subject of underwater acoustic communication in the spring semester of 2009 at the Norwegian University of Science and Technology (NTNU). After discussion with Professor Jens M. Hovem a study with simulations of underwater acoustic communication for sensor networks was proposed. I would like to thank Professor Jens M. Hovem for guidance and giving me the opportunity to work on a subject that I find very interesting. I would like to thank Xueshan Bao for help with the EasyPLR simulation program and for fixing the errors I found in the simulation program very fast. I would also like to thank Guosong Zhang and Anders Dale for helpful discussion concerning communication theory.

Trondheim, 1 July 2009

Ole Trygve Haug

Contents

Chapter 1

Introduction

Underwater wireless sensor networks have the possibility to be used in different applications both in civilian and military applications and therefore much research has been published the last decade about this subject. These sensor networks can be used for applications in military surveillance, seismic explorations for long time monitoring such as 4D-seismic and monitoring of the environment, especially when environmental accidents have happened.

These types of tasks may produce a large amount of data and the wireless sensor must be able to transmit this information. In terrestrial wireless systems radio waves are the most common choice, but underwater only radio waves with very low frequencies are able to propagate far through water.

Because of this problems most underwater sensor networks are based on acoustic waves. But the important limitation for underwater wireless acoustic sensor networks is that the speed of sound underwater is only approximately 1500 m/s. Compared radio waves that have a velocity of approximately $3 \cdot 10^8$ m/s it is not possible to transmit the same amount of information underwater with acoustic waves as it will be possible to do in terrestrial communication with radio waves. Another problem is the high amount of loss that makes it a challenge for long distance communications, especially for battery powered application with limited energy available.

For underwater communication with acoustic waves there are many challenges and choices that need to be done to make the system work properly. In this thesis an underwater acoustic communication system will be simulated and studied and the simulation program that is being used is called EasyPLR. The EasyPLR program is based on the PlaneRay propagation model that is presented in [15] and [16]. The EasyPLR program is a Matlab script and therefore all the programming and analysis will be done in Matlab. The EasyPLR program will also be modified to be able to handle different types of pulse-shapes and to be able to simulate modulated signals.

The problem with loss and how this affects the communication will also be looked into, and since loss is frequency dependent different carrier frequencies will be tested to see how this would affect the transmission-loss. Since the loss varies with the distance simulation of communication will be tested for different distances and evaluated.

Another important problem with underwater acoustic communication is that the sound speed varies with depth, but also with time and place. Especially the seasonal variations will give

variation in the sound wave propagation and this will give different results for the transmission of communication signals. To simulate this variation so called sound speed profiles will be used to vary the sound speed with depth. In the simulations the seasonal and geographical variations will be simulated by using different sound speed profiles from different locations and seasons. In the simulations of underwater acoustic communication phase shift keying will be used as the modulation technique. For systems with multiple users and to make the system more robust against disturbances multiple access methods should be used. And in this study direct sequence spread spectrum, that is used in Code division multiple access (CDMA), will be implemented and simulated in the underwater acoustic channel.

Chapter 2

The acoustic channel

The underwater acoustic (UWA) channel is quite different from the terrestrial radio channel in many aspects and has more challenges. The UWA channel is affected by noise, multipaths, transmission loss, Doppler spreading and variable delay. This makes underwater acoustic communication challenging and in next sections the these limitations that affects the communication will be discussed.

2.1 Noise

The noise sources in an UWA channels can be divided into ambient noise and man-made noise. The ambient noise is caused by biological creatures, seismic phenomenon and movement of water such as waves. The ambient noise often follows some curves called Knudsen curves. These Knudsen curves show that the ambient noise is being reduced as the frequency increases. According to the curves the ambient noise will be reduced with about 17 dB per decade of frequency, [14]. For high frequencies the thermal noise can be very dominating, especially over 100-200 kHz, where the thermal noise increases with 20 dB per decade. Another source of ambient noise is water bubbles that can affect underwater communication. According to [5] in the 10-20 kHz band the dominant noise source may be resonant air bubbles in the area near the surface. The resonant frequency f_0 is given by the following equation:

$$f_0 = \frac{1}{2\pi R}\sqrt{\frac{2\gamma P_0}{\rho}} \tag{2.1}$$

here γ is the ratio of specific heats, P_0 is the ambient pressure and ρ is the water density. The other source of noise is the so called man-made noise that may be caused by noise from ships, oilrigs and similar. This is especially an important noise source when UWA sensor networks (UWA-SN) is being used for 4D-seismic close to oilrigs.

2.2 Loss

Transmission loss is caused by attenuation and geometric spreading for signals that are transmitted directly to the receiver. Reflected signals will also have transmission loss due to the transmission coefficient, [14].

The geometrical spreading is caused by the movement of the wave-front, and for further distance the wave front is spread over a larger area. There are in general two types of geometrical spreading in underwater acoustic communication: Cylindrical and spherical. Cylindrical spreading is typical for shallow water UWA communication and has only horizontal spreading. Spherical spreading is typical for deep water UWA communication and can be seen as an omni-directional point source, [2].

Geometrical spreading will cause the acoustic intensity to decrease with increased distance. Cylindrical wave propagation results in the following geometrical spreading of the intensity I(r):

$$I(r)_{cylindrical} = \frac{p^2}{\rho c} = \frac{W}{2\pi r} \tag{2.2}$$

where W is the acoustic power and r is the distance from the source.

For spherical acoustic waves the wave front will spread as an increasing sphere. The intensity will decrease with the inverse square of the distance, called the *inverse square law*:

$$I(r)_{spherical} = \frac{W}{4\pi r^2} \tag{2.3}$$

The attenuation occurs because of absorption when acoustic energy is transformed into heat, and this will increase with both distance and frequency, [3]. The major factors for absorption are viscosity, thermal conductivity and other relaxation phenomena. Viscosity is the phenomenon of resistance against stress in a fluid. This is the major factor for absorption in freshwater. Thermal conductivity is another factor that affects the absorption in water. This effect occurs because volume changes creates heat that is being transferred away from the acoustic wave, and thereby reducing the energy in the wave. In seawater there are other relaxation phenomena that affect the absorption too. There are in general two relaxation processes that have a major contribution to the absorption. These relaxation processes involve boronic acid and magnesium sulphate, [14]. The total absorption of these contributions is given in equation 2.4, that is given by [8] and [9]:

$$\alpha = A_0 f^2 + A_1 \frac{f^2 f_1}{f_1^2 + f^2} + A_2 \frac{f^2 f_2}{f_2^2 + f^2} \tag{2.4}$$

Here A_0, A_1, and A_2 are constants, and f_1 and f_2 are the relaxation frequencies for boronic acid and magnesium sulphate. These relaxation frequencies and constants will depend on the temperature, pressure and pH value in the water. As seen from the equation the absorption will depend heavily on the frequency, and the absorption will increase for higher frequencies.

Reflection loss from the water surface will under calm condition give almost no loss, but if there a lot of waves there may be some loss. Reflection loss caused by sound waves hitting the bottom will depend on the sediment in bottom and the angle of the incoming sound wave. Very often the sound speed will be higher in the bottom than in water and part of the energy will be transmitted into the sediment layers. How much of the sound energy will be lost in the bottom and not be reflected will also depend on the frequency. Since underwater communication for high data rate will use a quite high carrier-frequency the loss will be large.

Air bubbles in the water will also affect the transmission heavily since the sound speed in air is much lower. Therefore under the right circumstances the air bubbles may almost block the sound wave passing through the bubbles.

2.3 Doppler spreading

Doppler spreading occurs because of Doppler shift of frequencies of different signal components. This may occur because of movement by the transmitter and the receiver. Signals reflected by the surface may also encounter this effect because of movement in the surface cause by waves. Doppler spreading will give a change of the transmission frequency and a continuous spreading of the frequencies, [3]. The change of the transmission frequency can be compensated for in the receiver, but the general spreading is harder to deal with. Doppler spreading is considered to be a huge challenge for the modulation techniques and the multi-channel access methods.

2.4 Multipath and time-delay

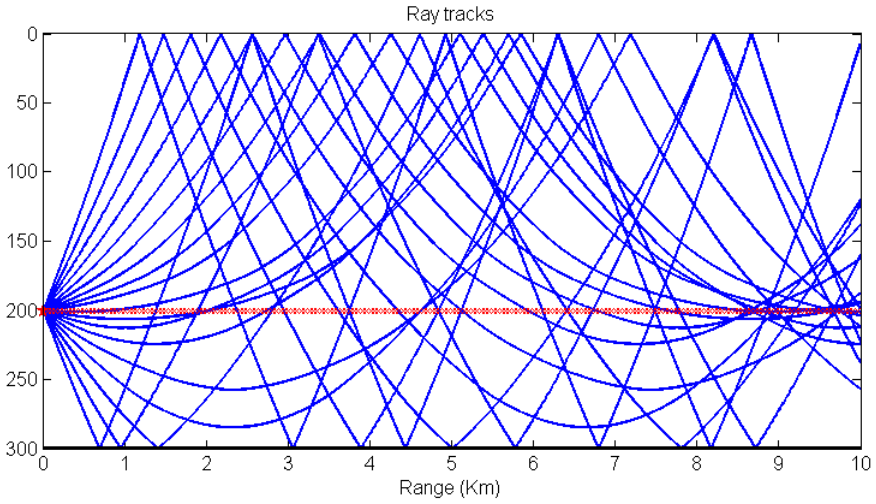

Figure 2.1: Ray tracing with different multipath.

Multipath is a huge problem that might affect the communication severely, and will give inter symbol interference (ISI). How much the multipath will occur depends on many physical factors, but the depth depended sound velocity is most important. In figure 2.1 this is illustrated for

an depth depended sound velocity that will give a bending of the sound rays in the horizontal direction, as described in [14]. The choice of spacing size between the sensors needs to take this effect into account. Another problem is that the depth depended sound velocity changes through the season and thereby change the multipath through the season making it harder to design the UWA-SN system.

This may lead to constructive or destructive interference. The received signal may be amplified or it may be reduced depending on the phase of different multipath. Multipath occurs because of reflection of waves from the surface and the bottom. The receiver will receive multiple signals, both direct, and reflected signals from the surface and the bottom. But there may also be several direct waves that may arrive at different times depending on how much the waves have been bend. Large time delay is caused by the fact that the sound speed under water is in the area of 1500 m/s, which is much lower than the speed of radio waves that is approximately $3 \cdot 10^8$ m/s. In terrestrial radio communication multipath and reflection will not be a problem since the delay is so little, but in UWA communication these delays may arrive very late and cause problem for the communication. This is further complicated by the fact that the delays may vary a lot.

Multipath may reduce the data transmission data severely, depending on how the receiver deals with different multipath. This will be discussed in section 3.3.

2.5 Sound speed

In general in acoustics the sound speed is given by the bulk modulus and the density of the medium. In the ocean these factors depends on the water temperature, salinity and the depth of the water. There exist several formulas for calculating the sound speed in water, and according to ref [14] the formula given by [12] should be accurate enough for the sound speed c given in m/s:

$$c = 1448.6 + 4.618T - 0.0523T^2 + 1.25(S - 35) + 0.017D \tag{2.5}$$

where

$$\text{T = temperature } (^\circ C) \text{ S = salinity (pro mille) D = depth (m)}$$

The sound speed will vary since the temperature, salinity and depth are of course varying factors. In figure 4.9 two sound speed profiles are given. The profile can be divided into several layers with different characteristics for the sound speed. The layer near the surface will have a sound speed that varies with daily changes and seasonal changes in the temperature in the water. But also because of waves the water masses will be changed and the sound speed will vary. Below the surface layer is the seasonal thermocline layer where the sound speed will decrease with depth because the temperature is decreased with increased depth. Here there is a distinctive difference between summer and winter, because this effect is greater during summer than winter. Under this layer the main thermocline layer where the temperature is also decreasing, but is not so affected by the conditions in the surface, and therefore the sound speed is decreasing more stabile. Below this layer is the deep isothermal layer where the temperature is almost constant, but the sound speed will increase with depth because of increased pressure. So between the

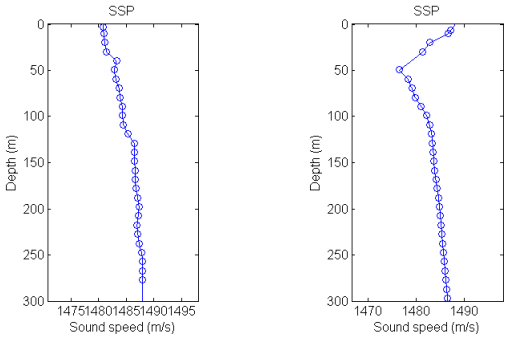

(a) Date: 19 February 2006 (b) Date: 08 June 1999

Figure 2.2: Different sound speed profiles for winter and summer.

main thermocline and the isothermal layer the sound speed will reach a minimum and this will create a sound channel. This sound channel has the ability to transmit low frequency signals very far. Where this minimum occurs will vary a lot from region to region. In the southern waters this minimum can be at 1000 meter, but northern waters it will be higher up. In polar areas this minimum will be much closer to the surface. In figure 4.9 sound speed profiles from the Norwegian Sea from winter and summer are shown. Here it can easily be seen how different the sound speed is change in the upper layer. This is because the temperature changes in upper layer through different seasons. The change in the sound speed will give refraction that will affect the communication.

2.6 Refraction

One important consequence of the variation in the sound speed underwater is the effect of refraction. Refraction means that the direction of the wave changes because of change in the sound speed. The refraction effect will occur every time the sound speed changes. For underwater acoustic rays this may lead to bending of the waves' direction so that the wave will not go in a straight line, as can be seen in figure 2.1. The water depth can be divided into different layers. Every time the sound speed changes for increasing depth a new layer is defined, and the refraction effect can then be described by Snell's law as:

$$\frac{\cos\phi_i}{c_i} = \frac{\cos\phi_{i+1}}{c_{i+1}} \tag{2.6}$$

where ϕ_i is angle between the layer and the incoming wave and ϕ_{i+1} is angle between the layer and the outgoing wave. c_i and c_{i+1} are sound speeds of the two layers.

2.7 Capacity

The capacity of a channel is given in [7] and is described in equation 2.7 as:

$$C = \max_{p(x)} I(X;Y) \tag{2.7}$$

Here is I(X;Y) the mutual information and for an additive white Gaussian noise channel (AWGN) equation 2.7 can, according to [7] and [11],be rewritten to equation 2.8:

$$C = Wlog_2\left(1 + \frac{P}{N_0 W}\right) \tag{2.8}$$

Here P is the power, and by using the relationship in equation 2.9:

$$P = E_b C \tag{2.9}$$

the following equation for the capacity C can be found according to [11] and [17]:

$$C = Wlog_2\left(1 + \frac{E_b C}{N_0 W}\right) \tag{2.10}$$

where E_b is the energy per bit, N_0 the noise spectral density and W is the bandwidth.

Distance	*Range*	*Bandwidth*
Very long	1000 km	less than 1 kHz
Long	10-100 km	a few kilohertz
Medium	1-10 km	20-50 kHz
Very short	less than 0.1 km	more than 100 kHz

Table 2.1: Bandwidth for different ranges in an underwater acoustic channel, given in [3] and [23].

Due to the mentioned limitations the available bandwidth for underwater acoustic communication will be severely limited, and it will depend on both frequency and range. This means that the available bandwidth will be much larger for short distance communication compared to long distance. In table 2.1 the available bandwidth is given for different range as described in [23] and [3]. Of course this can only be seen as an approximately bandwidth and will depend on many local factors.

Chapter 3

Channel modulation and multiple access methods

3.1 Modulation techniques

Modulation techniques can in general be divided into coherent and non-coherent methods. For use in underwater acoustic communication in the past most development in modulation techniques were based on non-coherent frequency shift keying (FSK). This was because non-coherent frequency shift keying relies on energy detection that is a robust method in the harsh conditions in the underwater acoustic channel. As mentioned in [2] the use of energy detection means that phase tracking is not necessary, which is a huge benefit in an underwater channel because of Doppler spreading that makes it quite difficult to track the phase. In underwater FSK modulation the problem with multipath effects is solved by inserting guard times between signal pulses to avoid disturbance from late arriving multipath signals. Dynamic frequency guards can also be used between frequency tones to adapt the communication to the Doppler spreading of the channel. Non-coherent modulation techniques such as FSK have high power efficiency but low bandwidth efficiency. For high data rate sensors this will be problem and coherent modulation techniques such as phase shift keying (PSK) and quadrature amplitude modulation (QAM) have been seen as the appropriate technique for high data rate sensor networks. Therefore extensive research has been done in this area.

The performance for different modulation techniques depends on several factors and there is a tradeoff between maximizing the bandwidth efficiency, given by R/W (bits/s)/Hz, and minimizing Signal-to-noise ratio (SNR). Here R is the data rate (bits/s) and the SNR is given by E_b/N_0. The reason for wanting to keep the SNR low is to reduce the energy consumption. In figure 3.1, given by [20], the performance in bandwidth efficiency for different modulation techniques are plotted as a function of the SNR value. And figure 3.1 illustrates the tradeoff between using high-level modulation that gives increased bandwidth efficiency and having a low SNR. For bandwidth-limited system the bandwidth efficiency should be $R/W > 1$, and for power-limited systems the bandwidth efficiency should be $R/W < 1$, [17]. The capicity limit of the channel will be C/W, as given in equation 2.10, and R will always be $R \leq C$.

In the simulations performed in this study Phase shift keying (PSK) will be used as modula-

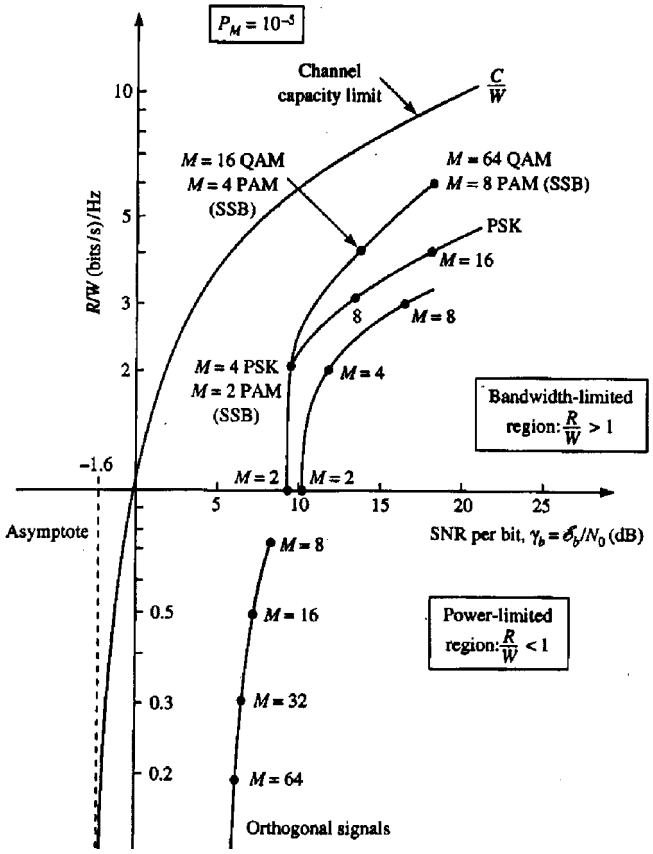

Figure 3.1: Bandwidth efficiency given in bit/s/Hz as a function of SNR per bit, as shown in [20]. FSK is given with bandwidth efficiency less than 1, and QAM, PAM and PSK is given with bandwidth efficiency greater than 1.

tion technique because of its high bandwidth efficiency and that it is not too complicated to implement. In the next section different types of Phase shift keying will be discussed.

3.1.1 Binary phase shift keying (BPSK)

The simplest form of phase shift keying (PSK) is binary PSK (BPSK) where only one bit is transmitted each time. The carrier wave will either have no phase shift or a phase shift of π radians. This will give the following pair of signals given in equation 3.1 and 3.2, [13]:

$$s_1(t) = \sqrt{\frac{2E_b}{T_b}} \cos(2\pi f_c t) \tag{3.1}$$

$$s_2(t) = \sqrt{\frac{2E_b}{T_b}} \cos(2\pi f_c t + \pi) = -\sqrt{\frac{2E_b}{T_b}} \cos(2\pi f_c t) \tag{3.2}$$

Here E_b the transmitted signal energy per bit. The time variable t varies from $0 \leq t \leq T_b$.

Since this modulation method only consists of two symbols there will only be one basis function, ϕ_1, given in equation 3.3.

$$\phi_1(t) = \sqrt{\frac{2}{T_b}}\cos(2\pi f_c t), \qquad 0 \leq t \leq T_b \tag{3.3}$$

By using this basis function the pair of signals, $s_1(t)$ and $s_2(t)$, can be rewritten to:

$$s_1(t) = \sqrt{E_b}\phi_1(t), \qquad 0 \leq t \leq T_b \tag{3.4}$$

$$s_2(t) = -\sqrt{E_b}\phi_1(t), \qquad 0 \leq t \leq T_b \tag{3.5}$$

These results can then be used to define the messages points for the signal space as:

$$s_{11} = \int_0^{T_b} s_1(t)\phi_1(t)\,dt \; = \sqrt{E_b} \tag{3.6}$$

$$s_{21} = \int_0^{T_b} s_2(t)\phi_1(t)\,dt \; = -\sqrt{E_b} \tag{3.7}$$

This means that the transmitter will vary between transmitting positive or negative values of a signal, depending on the input data. And in figure 3.2 a BPSK transmitter is shown with a very simple structure. Depending on the input bit the phase modulator will vary the phase between 0 radians and ϕ radians.

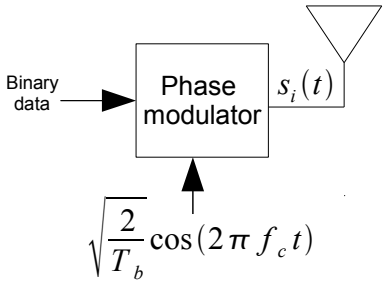

Figure 3.2: Binary phase shift keying transmitter

In the receiver shown in figure 3.3 the received signal will consist of the transmitted signal with some time delay T_d and some noise from the channel $n(t)$. The received signal will be multiplied with the basis function ϕ_1 and integrated over the symbol time period. This system is called a correlator. After the correlation process a decision device will decide if the received signal should be 1 or 0, depending on if the signal is positive or negative.

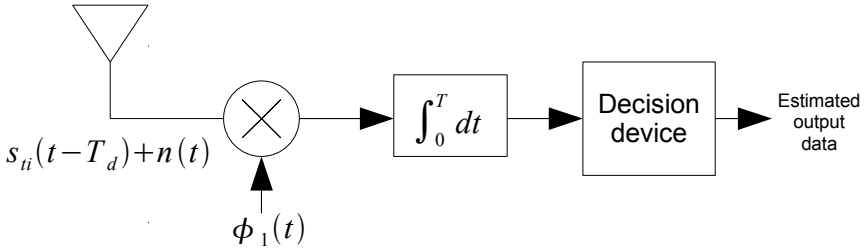

Figure 3.3: Binary phase shift keying receiver

3.1.2 Quadrature phase shift keying (QPSK)

The use of binary phase shift keying is not very effective since it is only able to transmit one bit each time. By using Quadrature phase-shift keying (QPSK) instead it is possible to send two bits each time. The basic idea is to let the carrier wave have four different phase values, one for each symbol. Here each symbol consists of two bits, such as 11. Normally the four phase values are $\pi/4$, $3\pi/4$, $5\pi/4$ and $7\pi/4$. By using these values the transmitted signal will be:

$$s_i(t) = \sqrt{\frac{2E}{T}}\cos(2\pi f_c t + (2i-1)\frac{\pi}{4}), \qquad 0 \le t \le T, \quad i = 1,2,3,4 \tag{3.8}$$

The equation 3.8 for s_i can be rewritten by using trigonometric identities to the following:

$$s_i(t) = \sqrt{\frac{2E}{T}}\cos(2\pi f_c t)\cos((2i-1)\frac{\pi}{4}) - \sqrt{\frac{2E}{T}}\sin(2\pi f_c t)\sin((2i-1)\frac{\pi}{4})) \tag{3.9}$$

Here t varies between $0 \le t \le T$ and i = 1, 2, 3, 4. From equation 3.9 it can be seen that the transmitted signal consist of two components that can be defined as channels called in-phase and quadrature-phase QPSK channels. This means that the signal consist of two basis functions with symbols $\phi_1(t)$ and $\phi_2(t)$. These basis functions are defined as:

$$\phi_1(t) = \sqrt{\frac{2}{T}}\cos(2\pi f_c t), \qquad 0 \le t \le T \tag{3.10}$$

$$\phi_2(t) = \sqrt{\frac{2}{T}}\sin(2\pi f_c t), \qquad 0 \le t \le T \tag{3.11}$$

These two basis functions will give four different message points in the signal space that is shown in figure 3.4.

These message points have the following signal vectors:

$$\mathbf{s}_i = \begin{pmatrix} \sqrt{E}\cos((2i-1)\frac{\pi}{4}) \\ -\sqrt{E}\sin((2i-1)\frac{\pi}{4}) \end{pmatrix}, \qquad i = 1,2,3,4 \tag{3.12}$$

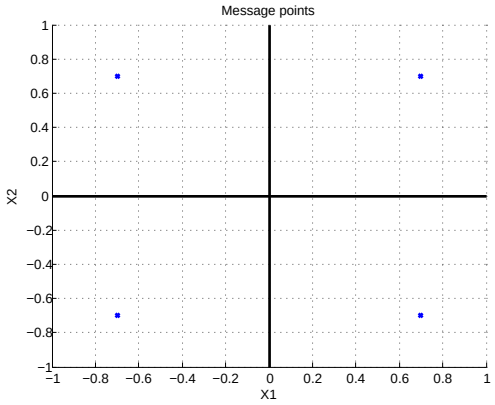

Figure 3.4: Signal space with message points for Quadrature phase shift keying.

In table 3.1 the coordinates for the different message points are shown together with their Gray-encoded input bits given by [13].

Binary symbol	*Phase*	S_{i1}	S_{i2}
10	$\frac{\pi}{4}$	$\sqrt{\frac{E}{2}}$	$-\sqrt{\frac{E}{2}}$
00	$\frac{3\pi}{4}$	$-\sqrt{\frac{E}{2}}$	$-\sqrt{\frac{E}{2}}$
01	$\frac{5\pi}{4}$	$-\sqrt{\frac{E}{2}}$	$\sqrt{\frac{E}{2}}$
11	$\frac{7\pi}{4}$	$\sqrt{\frac{E}{2}}$	$\sqrt{\frac{E}{2}}$

Table 3.1: Coordinates for different message points with Gray-encoded input bits

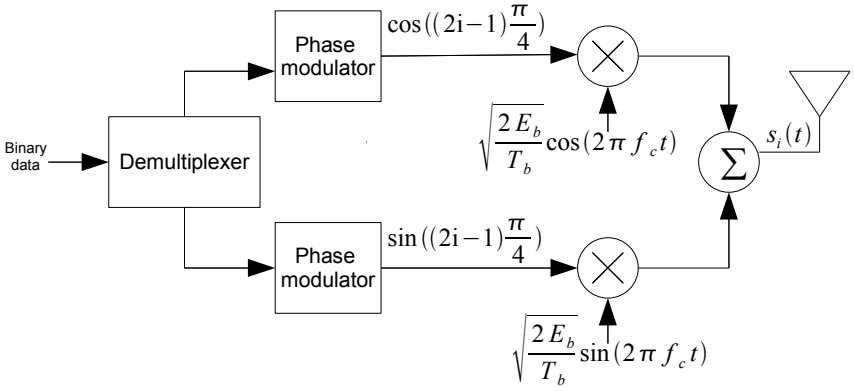

Figure 3.5: Quadrature phase shift keying transmitter

In figure 3.5 a block diagram of a common QPSK transmitter is shown. The binary data sequence is transformed into a polar form by a nonreturn-to-zero level encoder, where the binary symbols, 1 and 0, are represented with $\sqrt{E_b}$ and $-\sqrt{E_b}$. The next step in the generator is the demultiplexer that separates the binary symbols into two separate binary waves, s_{i1} and s_{i2}. These binary waves are multiplied with the basis functions $\phi_1(t)$ and $\phi_2(t)$ as given in equation 3.12. Then these two binary waves are added together to form the output signal $s_i(t)$, which is the final

QPSK signal. This signal can also be generated directly by changing the phase of the carrier, depending of the implementation choice.

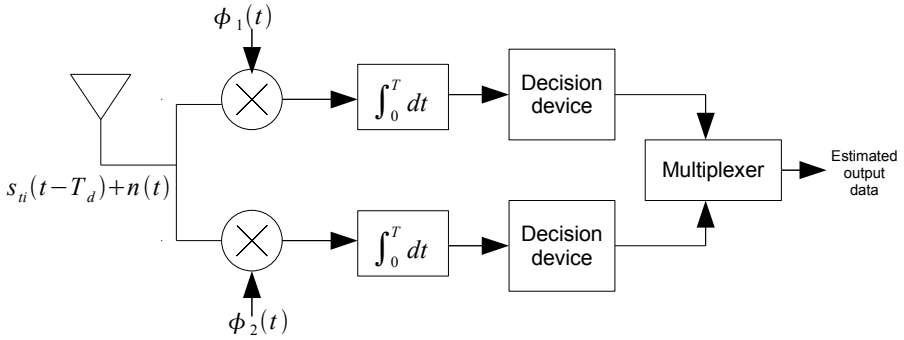

Figure 3.6: Quadrature phase shift keying receiver

After the signal is transmitted the QPSK receiver will use the same basis functions as in the transmitter. In figure 3.6 a block diagram of the receiver is shown. The received signal x(t) is used as an input to two correlators. These correlators consist of a multiplicator and an integrator. Each of these correlators uses one of the basis function, and this basis function $\phi_i(t)$ is multiplied with the received signal x(t). Then the product of the multiplication is integrated and the output signals of the correlators are x_1 and x_2. A decision device is then used to decide if the output values of the correlators are negative or positive. If $x_i > 0$ then the output bit is 1 and if $x_i < 0$ the output bit is 0. Since the receiver consists of two binary sequences, these two sequences are combined together in a multiplexer to produce the final symbol. This will symbol will have two bits, giving four different possible values. This symbol should consist of the two same bits as in the transmitter.

A general model for a received QPSK signal x(t) is given in equation 3.16.

$$x(t) = s_i(t) + w(t), \qquad 0 \leq t \leq T, \quad i = 1, 2, 3, 4 \tag{3.13}$$

By defining $x_1(t)$ and $x_2(t)$ as the output values of the correlators will give following result shown in equation 3.17 and 3.18:

$$x_1(t) = \int_0^T x(t)\phi_1(t)\,dt \;\; = \sqrt{E}\cos\Big((2i-1)\frac{\pi}{4}\Big) + w_1$$

$$x_1(t) = \pm\sqrt{\frac{E}{2}} + w_1 \tag{3.14}$$

For x_2 the result is similar:

$$x_2(t) = \int_0^T x(t)\phi_2(t)\,dt \;\; = -\sqrt{E}\cos\Big((2i-1)\frac{\pi}{4}\Big) + w_2$$

$$x_2(t) = \mp\sqrt{\frac{E}{2}} + w_2 \tag{3.15}$$

These equations shown that the input value to the decision devices will be positive or negative received energy value together with some noise.

According to [13] in a QPSK system the average probability of error in each channel is:

$$P_er = \frac{1}{2}erfc\Big(\sqrt{\frac{E}{2N_0}}\Big) \tag{3.16}$$

In a QPSK system the errors in the in-phase and quadrature channels have no correlation, meaning that they are independent of each other. Therefore the average probability of correct decision will be the product of the channels' average probability of correct decision:

$$\begin{aligned} P_c &= (1 - P_{er})^2 = \Big[1 - \frac{1}{2}erfc\Big(\sqrt{\frac{E}{2N_0}}\Big)\Big]^2 \\ P_c &= 1 - erfc\Big(\sqrt{\frac{E}{2N_0}}\Big) + \frac{1}{4}erfc^2\Big(\sqrt{\frac{E}{2N_0}}\Big) \end{aligned} \tag{3.17}$$

This will give an average probability of symbol error, P_e, for a QPSK system:

$$P_e = 1 - P_c = erfc\Big(\sqrt{\frac{E}{2N_0}}\Big) - \frac{1}{4}erfc^2\Big(\sqrt{\frac{E}{2N_0}}\Big) \tag{3.18}$$

Since the QPSK system is transmitting to bits per symbol the signal energy per symbol, E, is twice the signal energy per bit:

$$E = 2E_b \tag{3.19}$$

I situations where $(E/2N_0) >> 1$ and by using the average probability of symbol error, P_e can be simplified to:

$$P_e \simeq erfc\Big(\sqrt{\frac{E_b}{N_0}}\Big) \tag{3.20}$$

By using Gray encoding the bit error rate (BER) for QPSK is according to [13]:

$$BER = \frac{1}{2}erfc\sqrt{\frac{E_b}{N_0}} \tag{3.21}$$

This means that the QPSK system will have the same average probability for bit error as a binary PSK system (BPSK) for the same bit rate but only use half the bandwidth. So QPSK uses the bandwidth more efficient than BPSK and is therefore preferred.

3.2 Multiple access methods

For sensors that needs to send large amounts of data and for a network consisting of many sensors multiple access methods needs to be used. Several multiple access methods exist and are

being used in different wireless terrestrial applications where there are multiple users, but these techniques are not necessary suitable for underwater acoustic sensor networks (UWA-SN). In this study FDMA, TDMA and CDMA are being discussed and compared for use in underwater acoustic sensor networks:

- Frequency Division Multiple Access (FDMA) divides the frequency bands into subbands and gives each user a subband. FDMA are vulnerable to fading due to the fact that channels may be smaller than the coherence bandwidth of the transmission channel, [22]. Fading is a common problem in underwater wireless acoustic channels, but this problem can be solved by coding. This method can be very inefficient in bursty traffic due to fixed channel bandwidths and is not flexible if it is needed to do changes in the design. The narrow bandwidth, high variable delay and multipaths makes FDMA not suitable to UWA-SN, [2], [3], [19].

- Time Division Multiple Access (TDMA) divides time intervals or frames into time slots. To avoid collision of packets from close time slots guard times are used, which is proportional to the propagation delay. By using this technique TDMA needs more overhead than FDMA, [22]. TDMA sends information in bursts and the data is stored until its transmission time slot. So the transmitter can be turned off during none transmission periods and energy will be saved. Because the transmission occurs in bursts a high bit rate is required and there will be an increased ISI, and adaptive equalizers are needed. A huge advantage for TDMA is its flexibility because it does not need change of hardware to do changes. A major disadvantage is the need of strict synchronization. TDMA also need long time slots due to the long propagation delays in an underwater acoustic channel, and this gives low throughput. The variable propagation delay makes it difficult to design a precise synchronization system with a common timing reference needed for TDMA, [2], [19]. Due to the mentioned disadvantageous TDMA is not considered suitable for UWA-SN.

- Code Division Multiple Access (CDMA) let many users transmit over the whole frequency band at the same time. The different users' signals are separated by their unique pseudo noise (PN) spreading codes. CDMA modulates the information-signals by using orthogonal or non-orthogonal spreading codes. All the information signals that are modulated with the spreading codes will occupy the same bandwidth and time period. In the receiver the spread signals will be demodulated by using the spreading codes to separate the different signals, [11]. CDMA is a robust system that uses the bandwidth in an efficient way, and does not need strict synchronization, [24] . The problem of frequency selected fading that is caused by multipath is CDMA quite robust against since it has a large bandwidth and is able to distinguish among signals transmitted over the same bandwidth at the same time, [3] and [22]. There exist different forms of CDMA but the most common systems uses Spread Spectrum with Direct Sequence (DSSS) or Frequency Hopping (FHSS). Due to the mentioned disadvantages of FDMA and TDMA most literature today concludes that that CDMA is the most suitable and promising technique for use in UWA-SN, [2], [22], [3], [1], [6], [24], [19].

3.3 Code Division Multiple Access (CDMA)

As previous mentioned CDMA can be divided into Direct Sequence Spread Spectrum (DSSS) and Frequency Hopping Spread Spectrum (FHSS). In DSSS the transmitter multiplies the modulated signal $x(t)$ with the spreading code $S_c(t)$ that has a chip time T_c, and this can be seen in figure 3.7. The spread signal is than up-converted with a multiplication with the carrier wave $cos(2\pi f_c t)$ and transmitted in the channel $h(t)$, [11].

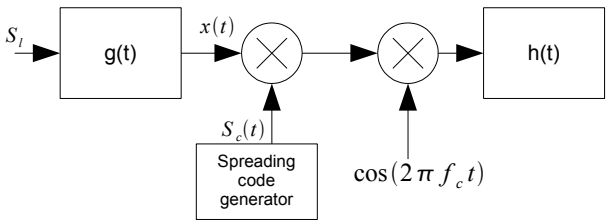

Figure 3.7: Direct sequence spread spectrum transmitter

In the receiver shown in figure 3.8 the received signal $r(t)$ is down-converted with $cos\,(2\pi f_c t + \phi)$, where ϕ is the matched phase to the incoming signal. The synchronizer is used to synchronize the spreading code generator with the incoming signal and the spreading code generator is used to despread the incoming signal with $S_c(t-\tau)$, and a matched filter $g'(-t)$ is employed to demodulate the signal.

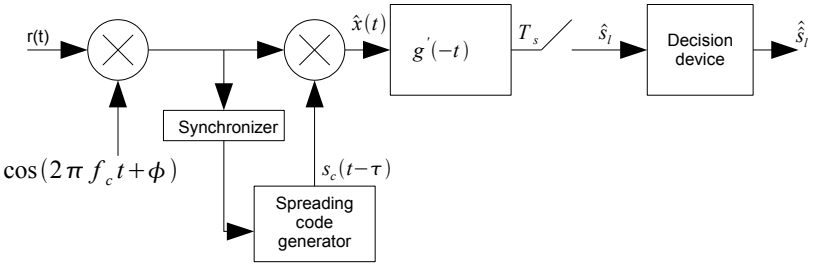

Figure 3.8: Direct sequence spread spectrum receiver

A DSSS system's fine time resolution of spreading codes provides possibility to coherently combine the multipath arrivals by using Rake receiver. The Rake receiver, shown in figure 3.9, consist of many branches that will synchronize to different multipath component, [4], and by using a Rake receiver other signals will be threaded as noise, which is a huge benefit. If the resolvable multipath components fade independently, it is possible to extract a time diversity gain present in the channel, [3], [22]. Another advantage because of this is that CDMA reduces the packet retransmissions and increases the reuse of the channel, and this will reduce the energy consumption in the batteries and increase the throughput.

In Frequency Hopping Spread Spectrum (FHSS) the carrier frequencies for the different information signals are changed in a pattern given by the unique spreading codes. The transmitter

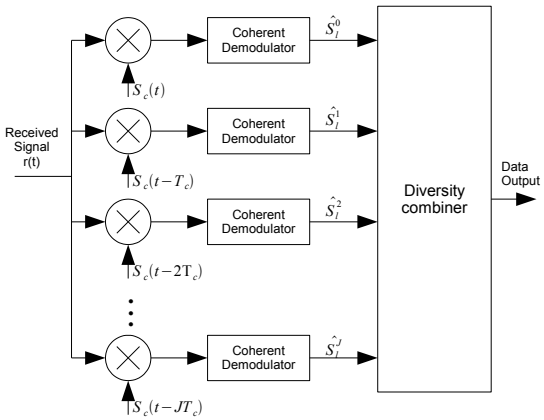

Figure 3.9: Rake receiver

is illustrated in figure 3.10 , and the spreading code is used as input to the frequency synthesizer that will generate a hopping carrier signal $cos(2\pi f_i t + \phi_i(t))$, [11]. This hopping carrier signal is then used as an input to the modulator to up-convert the information signal to the carrier frequency.

In the receiver that is given in figure 3.11 the received signal is used as an input to the synchronizer to synchronize the spreading code generator with the received signal. The spreading code $S_c(t-\tau)$ is used as an input to the frequency synthesizer to generate an hopping carrier signal that is used for down-conversion in the demodulation process, [11].

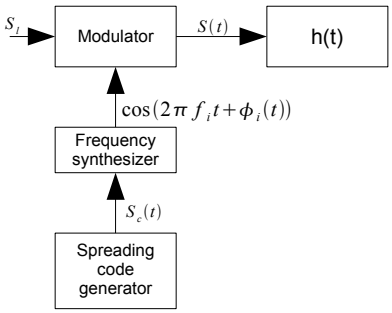

Figure 3.10: Frequency hopping spread spectrum transmitter

Frequency Hopping Spread Spectrum (FHSS) that has frequency bands separated by more than the coherence bandwidth will fade independently, and a coding scheme can be used to extract a diversity gain from the fading channel, [22].

The capacity in CDMA is limited by multiple access interference (MAI) that is caused by signals of other users that are overlapping in both time and frequency, due to the use of spread spectrum. In DSSS the MAI is caused by all users, and the total noise will be increased. In FHSS the MAI occurs because of the hopping pattern is interfered by the hopping pattern of other users. To reduce the MAI effect the FHSS can use codes with large spreading gains and also multiuser

receivers can be used. Transmitting in burst can increase the number of users, but additional users will increases the total interference so the system may perform worse.

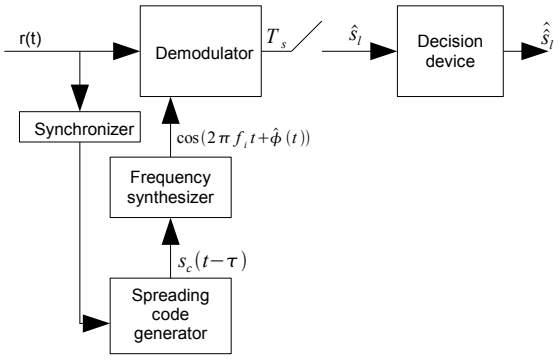

Figure 3.11: Frequency hopping spread spectrum receiver

By using non-orthogonal spreading codes there is no hard limit on the number of channels, but increased number of user will increase the interference between the users. CDMA is vulnerable to the near-far problem and to compensate for this problem non-orthogonal CDMA needs to use a power control algorithm. The power control will invert the attenuation and fading affecting the channel, and this will eliminate the near-far problem since each interferer will give an equal amount of power, [11], [22]. By using a power control algorithm the interference between different sensor nodes will be reduced. This will also reduce the general energy consumption which is a desirable effect for wireless battery powered sensors.

By using CDMA as the desired transmission technique it needs to be decided if Direct Sequence (DSSS) or Frequency Hopping (FHSS) CDMA should be chosen. In [10] the two transmission techniques PSK DSSS and FSK FHSS are being studied. The choice between these two techniques depends on their performance in multiuser systems and the impact of the underwater channel. DSSS' limited by the temporal coherence of the channel affect the maximum spreading factor that may make FHSS better alternative. The multipath resolving properties of DSSS minimize the effects of frequency-selective fading that is reducing the performance of FSK modulation.

For a DSSS system the spreading rate is increased with higher number of chips per data symbol, which will lead to an improvement of the SNR per symbol in additive white Gaussian noise (AWGN). For time-varying channels the gain depends on the stability of the channels environment that the wave propagates in. The gain of the receiver will be reduced if the channel changes considerable during one symbol period, and then the gain of the receiver will be reduced. This will result in a net loss when the length of the spreading code is increased past a certain point.

Which one of DSSS and FHSS that performs the best depends on the characteristics of the acoustic channel. In the simulation done in [10] the primary limitation was the time variability. DSSS performs very well when coupled with a chip rate equalizer. The variation in the channel gives the limitation of the performance of the receiver at high spreading rates.

FHSS is more vulnerable to the Doppler shift effect because the signals are transmitted in narrow bands, but more robust to multiple access interference (MAI) than DSSS. FHSS has a higher

Bit error ratio (BER) than DSSS, though FHSS has simple receivers and gives robustness to the near-far problem especially when used with convolution coding and soft-decision Viterbi decoding, thus simplifying the power control functionality, [2]. But the performance for FHSS is limited in frequency-selective channels.

In DSSS the received signal is multiplied with the original pseudo noise code and integrated over the period on the data symbol, also known as despreading. The despreading will decorrelate the MAI made by multiple signals. The problem with this method is that it has a very high complexity and therefore can be a problem to implement in small sensor with limited power, [3].

Even though there are advantageous and disadvantageous for both direct sequence spread spectrum (DSSS) and frequency hopping spread spectrum (FHSS) the DSSS has the best performance in underwater acoustic communication, [10]. Therefore DSSS is chosen as the spread spectrum technique for the simulation in this study.

3.4 Spreading codes

The spreading code c(t) is used to spread the signal in a spread spectrum systems. In direct sequence spread spectrum the spreading code will normally have values of 1 and -1. These values are normally generated through a system of shift registers. These shift registers will consist of values in a linear or non-linear combination of values from previous time intervals. When the spreading codes are used in a multiple access system the spreading codes needs to have good cross correlation. In situations where jamming is a problem the spreading waveform c(t) will have very long periods to avoid this problem. In a ideal situation the spreading code should have infinite length of random numbers, [18]. But this is not possible due to the limitation of the systems, such as storage and power consumption. Therefore the spreading codes uses so called periodic pseudorandom codes (PN codes). The theoretical background for PN codes is very complex and will not be explained in detail in this study, more detailed description of PN codes can be found in [18]. There exist several spreading code such as maximal-length code, Kasami codes and Gold codes.

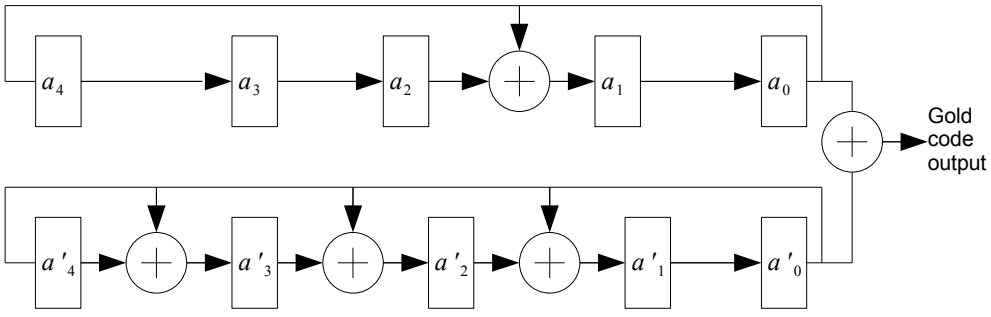

Figure 3.12: Gold code generator

In this study Gold codes have been chosen to be used in the simulations of direct sequence spread spectrum (DSSS). And in figure 3.12 a typical Gold code generator is shown. The advantage of Gold codes is that they have good cross-correlation properties. In multiple access systems such

as DSSS the interference between users with different spreading codes will depend heavily on how good the cross-correlation properties between the spreading codes are. Ideally at a given receiver only the wanted signal should be despread and signals with other spreading codes should not be depsread at all. Thereby the other signals will almost not affect at all the wanted signal. But since a real system is not ideal there will always be some disturbance from other signal. But how severe this disturbance is depends a lot on the spreading codes.

To understand Gold codes a m-sequence should be considered that is represented with a binary vector **b**, a another sequence **b'** that is generated through sampling every rth symbol of **b**, as given in [18]. The sequence **b'** has normally the notation **b'** = **b**$[r]$. This means that **b'** has been sampled every r'th time. The purpose with these definitions is to find preferred pairs of m-sequences. These preferred pairs of m-sequences have three valued cross-correlations spectrum, and the code period is $N = 2^n - 1$. For **b** and **b'** to be a preferred pair the following conditions need to be fulfilled, according to [18]:

- $n \neq 0 \mod 4$.This means that n is either odd or n = 2 mod 4.
- **b'** = **b**$[r]$, and r has to be odd and either: $q = 2^k + 1$ or $q = 2^2k - 2^k + 1$
- gcd (n,k) = $\begin{cases} 1 & \text{for n odd} \\ 2 & \text{for n} = 2 \mod 4 \end{cases}$

where *gcd* means *greatest common divisor*.

By having $b(D)$ and $b'(D)$ as preferred pair of m-sequences with code period N will give a set of Gold codes on the form:

$$\{b(D), b'(D), b(D) + b'(D), b(D) + Db'(D), b(D) + D^2b(D), ..., b(D) + D^{N-1}b'(D)\}$$

For more detailed explanation see [18].

3.5 Pulse shaping

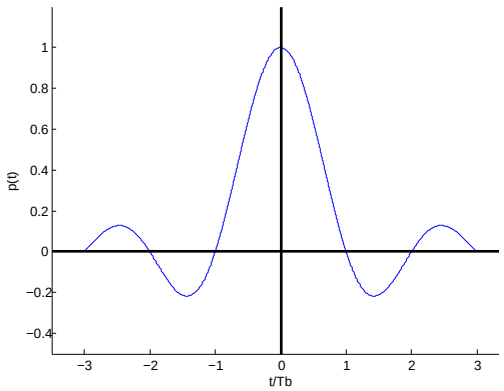

Figure 3.13: Sinc pulse

In band-limited channels the frequency bandwidth of the signal is limited and this will affect the shape of the pulse-signal. How the shape of the pulse is designed is important to avoid

intersymbol interference. Intersymbol interference (ISI) occurs when a symbol causes disturbance to the next symbol. Because of ISI there will be a tradeoff between how much band-limited the channel can be in the frequency domain and how the shape of the pulse will be in the time domain.

In an ideal Nyquist channel the signal pulse will be a rectangular function in the frequency domain, as shown in equation 3.22, [13].

$$P(f) = \begin{cases} \frac{1}{2W} & -W < f < W \\ 0 & |f| > W \end{cases} \tag{3.22}$$

By using a rectangular function, rect(f), this equation can be rewritten to:

$$P(f) = \frac{1}{2W} rect\left(\frac{f}{2W}\right) \tag{3.23}$$

The bandwidth off this signal is then:

$$W = \frac{R_b}{2} = \frac{1}{2T_b} \tag{3.24}$$

where T_b is bit duration and R_b is the bitrate. The time function can be found by inverse Fourier transformation of the frequency function. This will then give a sinc function:

$$p(t) = \frac{\sin(2\pi Wt)}{2\pi Wt} = sinc(2Wt) \tag{3.25}$$

The signal pulse in the time domain can be seen in figure 3.13. This pulse shape can also be a sinc filter. There are several disadvantageous by using a sinc shaping filter. The rectangular function in the frequency domain is not physical realizable, [13], because of the sharp edges. Another problem with the sinc function in the time domain is that the function has a slow rate of decay. This is caused by the lack of continuity at the maximum and minimum frequency (+/- W).

Due to the mentioned disadvantageous with the sinc filter there exist several other functions that are being used in pulse shaping filters. Examples of these functions are Gaussian, raised cosine and squared raised cosine.

3.5.1 Gaussian pulse shaping

The Gaussian pulse shaping filter is designed to minimize the rise and fall time. This filter is used in the Gaussian minimum shift keying (GMSK) that is a part of the Global System for Mobile Communications (GSM). The pulse shape of the Gaussian function in the frequency domain is given in [13] as follow:

$$H(f) = \exp\Big(-\frac{log2}{2}\Big(\frac{f}{W}\Big)^2\Big) \tag{3.26}$$

In the time domain this pulse shape will then be:

$$h(t) = \sqrt{\frac{2\pi}{\log 2}} W \exp\Big(- \frac{2\pi^2}{\log 2} W^2 t^2 \Big) \tag{3.27}$$

The motivation for using Gaussian pulse shaping in GMSK is based on some limitations in minimum shift keying (MSK). The most important factor in MSK that needs to be improved is to make the power spectrum more compact, and this is done by using a Gaussian pulse shape. Another advantage with a Gaussian pulse shape is relative low overshoot.

3.5.2 Raised cosine pulse shaping

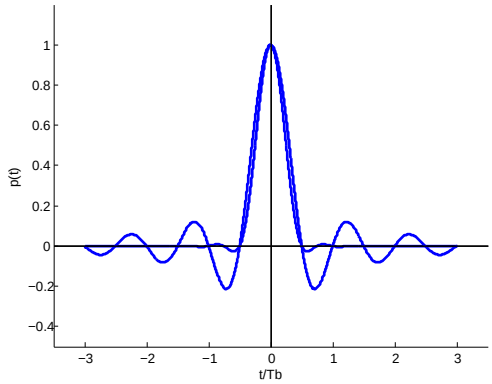

Figure 3.14: Raised cosine pulse

One of the most common pulse shapes in communication is the so called raised cosine pulse shape. This pulse has many similarities to the ideal Nyquist channel pulse but has some modifications to deal with the lack of continuity at the maximum and minimum frequency. The frequency response to the pulse shape P(f) is defined in equation 3.28:

$$P(f) = \begin{cases} \frac{1}{2W} & 0 < |f| < f_1 \\ \frac{1}{4W}\Big(1 - \sin\Big(\frac{\pi(|f|-W)}{2W-2f_1}\Big)\Big) & f_1 \leq |f| < 2W - f_1 \\ 0 & |f| \geq 2W - f_1 \end{cases} \tag{3.28}$$

The frequency variable f_1 is given by the *rolloff factor*, α, that indicates the excess bandwidth for the ideal bandwidth W is defined as:

$$\alpha = 1 - \frac{f_1}{W} \tag{3.29}$$

The transmission bandwidth B_T is defined as, [13]:

$$B_T = 2Wif_1 = W(1 + \alpha) \tag{3.30}$$

By choosing a rolloff factor of $\alpha = 0$ will give a rectangular frequency response P(f) in equation 3.28 with no continuity at the edges. But by changing the rolloff factor to $\alpha = 0$ there will be continuity at the maximum and minimum frequency. By use of inverse Fourier transform the pulse shape in the time domain can be found:

$$p(t) = sinc(2Wt)\Big(\frac{\cos(2\pi\alpha Wt)}{1 - 16\alpha^2 W^2 t^2}\Big) \tag{3.31}$$

As mentioned a roll off factor equal to zero will give a rectangular frequency response and the pulse shape g(t) can then be simplified to a sinc function:

$$p(t) = sinc(2Wt), \qquad for \alpha = 0 \tag{3.32}$$

By instead choosing $\alpha = 1$ to have more continuity in the frequency response the pulse shape will then be:

$$p(t) = \frac{sinc(4Wt)}{1 - 16W^2 t^2} \tag{3.33}$$

In figure 3.14 the pulse shape with rolloff factor of $\alpha = 0.1$ and $\alpha = 1$ is shown. It can there be seen that a rolloff factor of one will give a pulse shape that reduces more rapidly. Due to the mentioned reasons a rolloff factor equal to 1 will be used in the simulation in this study that uses raised cosine pulse shape.

3.5.3 Square-root raised cosine

To deal with the problem of white noise matched filters can be used, where the product of the transmitter filter and the receiver filter must be H(f). To deal with this problem so called square-root raised cosine filter can be used that is the square root of raised cosine. The pulse shape of this filter is defined as:

$$p(t) = \frac{\sin(2\pi Wt(1-\alpha)) + 4\alpha 2Wt\cos(2\pi Wt(1+\alpha))}{2\pi Wt(1-(4\alpha 2Wt)^2)} \tag{3.34}$$

3.5.4 Ricker wavelet

A pulse shape that is not common in communication systems is the so called Ricker wavelet or Mexican hat wavelet, shown in figure 3.5.4. The Ricker wavelet is a common pulse to use in seismic exploration, as described in [21]. In the EasyPLR program (described in section 4.1) the Ricker wavelet is used as the standard pulse and has the following function:

$$p(t) = (1 - 2(f\pi t)^2) \times \exp(-(f\pi t)^2) \tag{3.35}$$

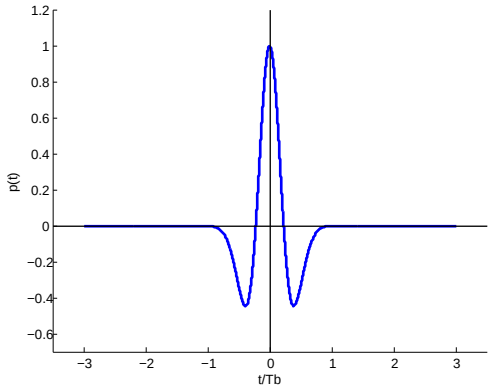

Figure 3.15: Ricker pulse

3.6 Ray tracing

For simulating wave propagation there exist several methods and in this study the simulations will be performed with a program based on ray tracing. The idea of ray tracing is that the sound waves will follow a various number of rays with paths that is normal to the wave-fronts. A short explanation is presented here and for more details see [14].

With rectangular coordinates the wave equation can be described with the two following equations:

$$\nabla^2 A - A\frac{\omega^2}{c_0^2}\nabla W \cdot \nabla W = -A\frac{\omega^2}{c^2} \tag{3.36}$$

$$2\nabla A \cdot \nabla W + A\nabla^2 W = 0 \tag{3.37}$$

To solve these equations some assumption can be done. By assuming that the frequency is of size where variation of the sound speed over a wavelength is very small, and that the spatial variation in the amplitude is very little the equations can be simplified to:

$$\nabla^2 A \ll A\frac{\omega^2}{c^2} \tag{3.38}$$

and equation 3.36 can be simplified to the **eikonal equation**

$$\nabla^2 W^2 = \left(\frac{c_0}{c}\right)^2 \tag{3.39}$$

Equation 3.37 is called the **transport equation** and shows the amplitude of the sound field. And Eeuation 3.39 gives the spatial variation of the wave-front.

By assuming that the sound speed is independent of horizontal distance and that it only varies with vertical distance some simplifications can be done. Since the sound speed is only varying in the horizontal direction Snell's law can be used to describe the change in the ray tracing parameters given in equation 3.40.

$$\xi = \frac{\cos\theta_0}{c_0} = \frac{\cos\theta\,(z)}{c\,(z)} \tag{3.40}$$

The different rays will follow the direction given by Snell's law in equation 3.40 and the propagation will follow curved paths where the radius of the curvature is given by $R = \frac{ds}{d\theta} = \frac{1}{\sin\theta}\frac{dz}{d\theta}$, and this gives:

$$R\,(z) = -\frac{1}{\xi g\,(z)} \tag{3.41}$$

Here $g\,(z)$ is the sound speed gradient.

To calculate the acoustic intensity the assumption is that the energy between two rays that have an initial separation $d\theta_0$ is constant. Based on this assumption the acoustic intensity as a function of distance can than be given as:

$$I\,(r) = I_0 \left(\frac{r_0^2}{r}\right)\left(\frac{c_0}{c}\right)\left|\frac{\cos\theta}{\sin\theta}\frac{d\theta_0}{dr}\right| \tag{3.42}$$

Chapter 4

Simulations and results

4.1 Simulation program

In the simulations done in this study the EasyPLR program is used that is based on the PlaneRay propagation model that is presented in [15] and [16]. The purpose of the EasyPLR program is to make the PlaneRay model easier to use. The PlaneRay propagation model is based on ray tracing and uses a unique sorting and interpolation routine. The model can also handle distance variations in the seafloor. The model is programmed in Matlab

The simulation results in the EasyPLR program will be organized with plots of ray tracing and different types of transmission loss. At a given receiver location the program will also give plots of the received pulse, time-delay, frequency spreading and eigen-ray distribution.

The EasyPLR program will for a given sound speed profile generate horizontal layers where the sound speed in each layer is given by the sound speed profile. The refraction or bending of the rays will use Snell's law given in equation 3.40 with sound speeds given by the input sound speed profile.

In the program it is possible to decide the beam-width and how many rays that is being used. The carrier frequency can also be specified. The depth to the seafloor and at what depth the transmitter can be placed at is specified by the user. The array of the receiver can be, if wanted, be placed at another depth than the transmitter, and the spacing between the receivers is given by the user.

In the receiver the different rays will be divided into different types of eigen-rays. Different types of eigen-rays are direct waves (with refraction), bottom reflected waves, surface reflected waves and waves reflected from both the surface and the bottom. These rays are interpolated together to give the different eigen-rays. The user will then for example only see one bottom reflected wave instead of all four bottom reflected waves. This makes it much easier to get the overview over the different types of waves.

The transmission loss will be calculated from: intensity with the assumption of constant energy between the rays, absorption in the water defined as dB/m and absorption because reflection loss defined as dB/λ

The time delay plot will use a theoretical direct wave with no refraction to use as the ray received at zero time. The time delay is then calculated as the difference in arriving time between this non-existing ray and other arriving rays. The time spread between to rays can be found by the difference in their separate time-delay.

In this simulation different input pulses are used and also the carrier frequency is varied. The maximum amplitude is at 200 Hz for all simulations. The seafloor is hard with a bottom density of 2000 kg/m^3 and a sound speed in the seabed of 1700 m/s. The bottom roughness was set to 0.1 m and the reflection loss was 1 dB/λ.

The number of rays was set to 700 to get high accuracy, but this needed to be reduced for some situation because it created waves that didn't exist. Different sound speed profiles were used for different simulations.

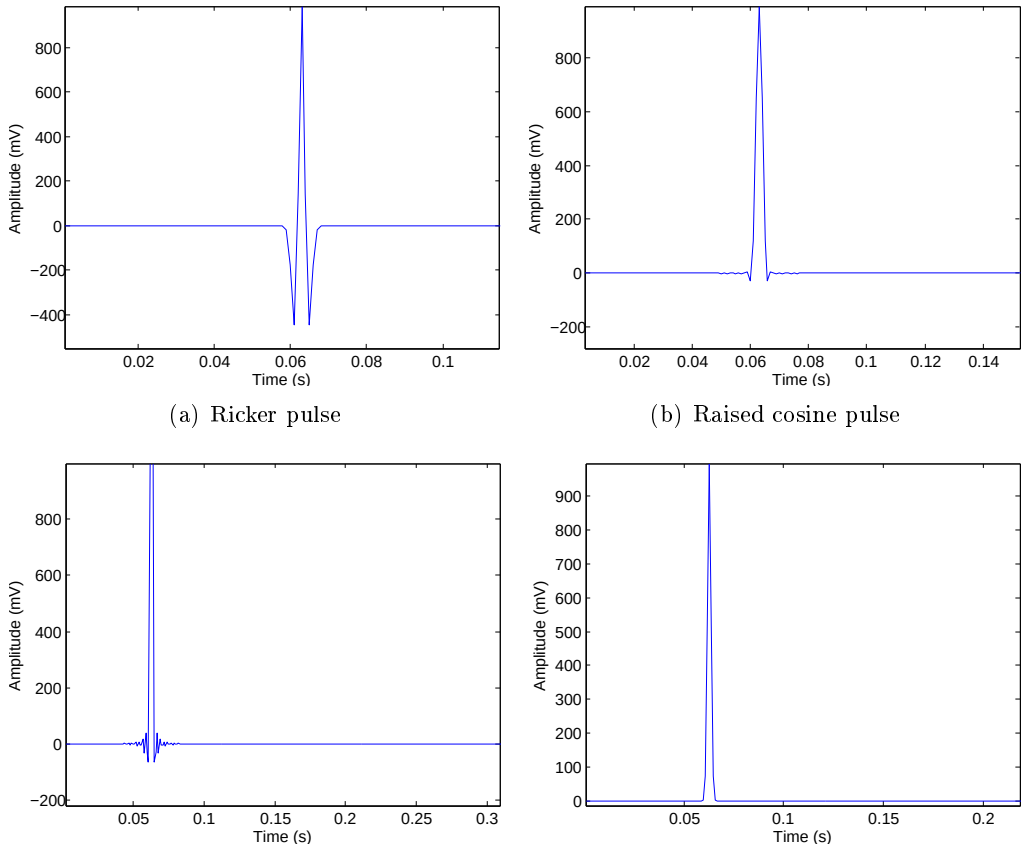

(a) Ricker pulse

(b) Raised cosine pulse

(c) Square raised cosine pulse

(d) Gaussian pulse

Figure 4.1: Different pulse shapes used in the EasyPLR simulations

The beam-width in this simulation was set to 20° that is the standard for this program. Varying the beam-width will give different results, but this was not analyzed since it is outside scope of this study.

The depth level was set to a total of 300 m with the transmitter at 250 m. The receivers were placed in an array at 250 m with spacing of 10 m. The reason for placing the transmitter 50 m over the seafloor was to get better transmission compared to having the transmitter at the

seafloor where it will give many bottom reflected waves and reduce the transmission capacity.

The EasyPLR program has been modified to be able to simulate underwater communication with modulation techniques. The EasyPLR program only has one type of pulse shape, the Ricker pulse described in section 3.5.4, and therefore it has been modified. Further modifications were needed to be done to make the program able to handle modulated signals. Through this semester there have been found several errors in the EasyPLR program giving wrong results and these have been corrected. It can never be guaranteed 100 percent that there is no errors left, but the version of EasyPLR that exist today gives much more correct results than the version that was available when the work started with this study.

4.2 Different types of pulses

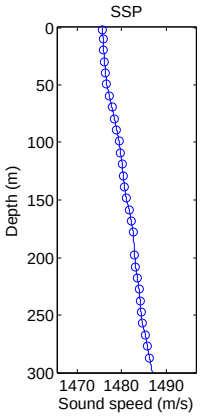

Figure 4.2: Sound speed profile measured at date 05 March 1997, at latitude 63.9172° and longitude 7.8967°

After initial testing of the program different pulses were used as input pulses in the EasyPLR program with a carrier frequency of 35 kHz. The different pulses that were tested were Ricker pulse, Raised cosine pulse, Square raised cosine pulse and Gaussian pulse. In section 3.5 these four pulses were described in detail and their different advantageous were mentioned. In this simulation the motivation was to see if there were any differences in the different pulses' performance. In figure 4.1 the four different input pulses to EasyPLR are shown. The sound speed profile that was used in this simulation is given in figure 4.2 and does not have any sudden change in sound speed. The distance to the receiver were changed, but no clear difference could be found between the different pulses, except from their frequency spectrum. At a distance of 1000 m the received pulses had the exact time-spread and the eigen-rays were the same.

In figure 4.4(a) the eigen-rays are shown for a receiver placed at 1000 m. This result is the same for all the four different pulses. The time-spread result is also the same for all the four different pulses and in figure 4.4(b) the time spread is shown for a receiver at 1000 m. At this position the time- spread between the direct wave and the bottom reflected wave is 0.178 ms.

Looking at the four different received pulses at 1000 m in figure 4.5 there is no major difference in the results for the received pulse shapes, except for the square raised cosine pulse. The square

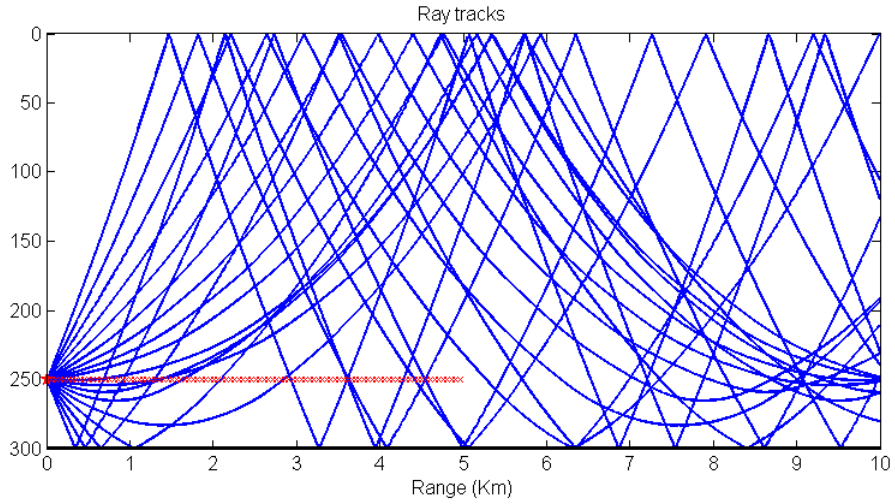

Figure 4.3: Example of ray tracing generated by EasyPLR. In the actual simulations a much higher number of rays were used.

raised cosine pulse is shown in figure 4.5(c) and has some oscillation effect in the signal and this is not suppose to be there. This effect may be caused by the so called Gibbs phenomenon or by some error in the programming of the transmitter filter. But since the pulse shape was not going to be used in further simulations this was not a major problem.

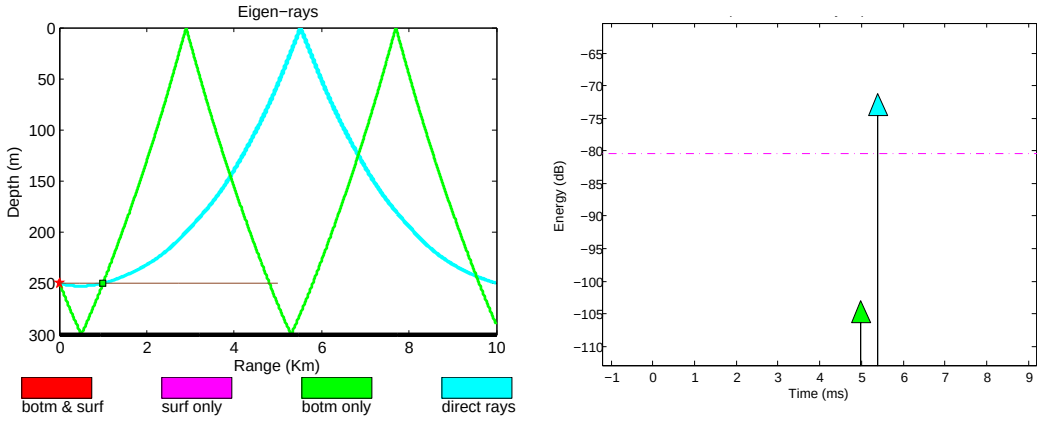

(a) Ricker pulse

(b) Raised cosine pulse

Figure 4.4: Eigen-rays and time-delay for the pulse shapes in figure 4.1

All the four received pulses at 1000 m consist of a direct wave and a bottom reflected wave. The direct waves have experienced a 90° phase shift because the wave is going through a so called turning point. This means that wave changes direction from going downwards to going upwards or from going upwards to going downwards. The second pulse shape in the received pulse is a bottom reflected pulse that has a 180° phase shift because it got reflected from the seafloor. This is same result for all the four cases, the only difference is the shape of the pulse. This is of course a result because the transmitted pulses had different shapes. The Ricker pulse was only used in this comparison because it is the standard pulse and is not interesting in a communication

system since the other pulses uses have better frequency spectrum for a communication system, as described in section 3.5.

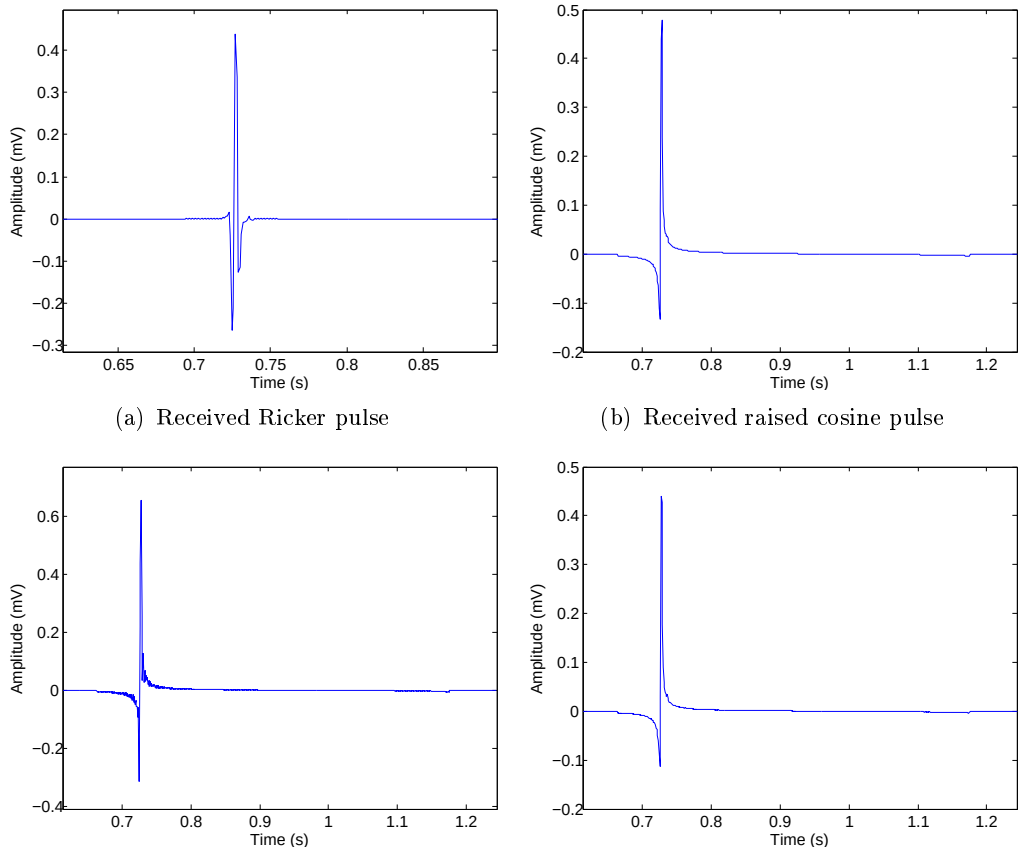

(a) Received Ricker pulse

(b) Received raised cosine pulse

(c) Received square raised cosine pulse

(d) Received Gaussian pulse

Figure 4.5: Received pulses at hydrophone location 1000 m with sound speed profile given in figure 4.2.

The EasyPLR program gives also result for three different types of loss; absorption loss, reflection loss and spreading loss. These three types of losses are given separate. For each type of loss the program will give the loss to the direct waves, the bottom reflected waves, the surface reflected waves and for waves reflected by surface and bottom. For the four different pulses there are no difference in the loss as expected and in figure 4.6 the different types of loss is plotted. These results are valid for all the four different pulse shapes.

For the absorption loss it increases with distance as expected and the reflected waves have higher loss than the direct waves. This is logical since the reflected waves have a longer travelling distance for increased horizontal distance than the direct waves that are only refracted. Since the transmitter is located only 50 meters from the bottom the bottom reflected waves will have lower loss than the surface reflected waves, since the horizontal distance to the surface is 250 m.

The direct waves will not have any reflection loss since they are not reflected. The bottom reflected waves will have quite high loss because they are reflected from bottom that is quite absorbing. The reflection loss for the surface reflected waves and for the waves reflected by both

the surface and the bottom will not be existing for shorter distance since they are not reflected to the hydrophones at this distance. They are first observed at almost 4 km. The spreading loss will as expected increases with distance since the sound waves will have some sort of spherical spreading at deep waters. All the types of waves will experience this for increasing distance.

For the rest of the simulations the raised cosine pulse is chosen as the transmitter pulse since this is the most common pulse shape in communication systems and the other pulses did not perform any better than the raised cosine pulse. But the square raised cosine pulse and the Gaussian pulses are good alternatives to be used, especially square raised cosine for use in matched filters.

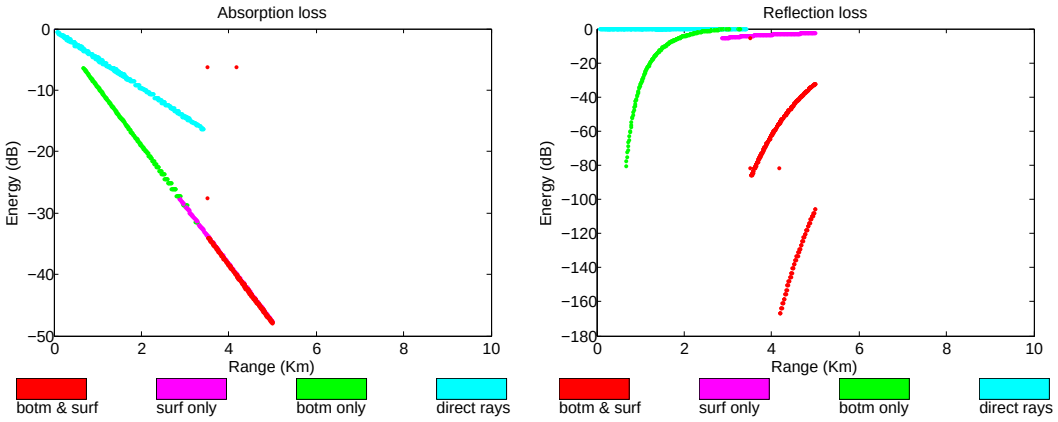

(a) Absorption loss

(b) Reflection loss

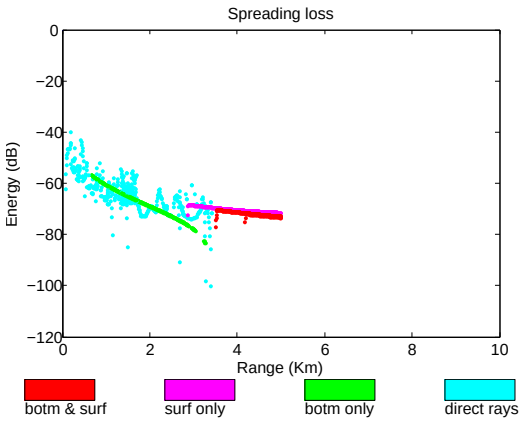

(c) Spreading loss

Figure 4.6: Different type of loss calculated by EasyPLR for the pulse shapes in figure 4.1 Different colors indicates loss caused by different factors. Loss caused only by surface (surf, red), only bottom (botm, green), bottom and surface (botm & surf), direct wave (blue).

4.3 Different carrier frequencies

In the previous simulations the carrier frequency has been chosen to be 35 kHz and this was mostly based on published studies that had good results for carrier frequencies around this area.

As described in section 2.2 the loss for underwater acoustic waves will depend heavily on the frequency. The absorption is severely dependent on the frequency as can be seen in equation 2.4. How much of the wave energy that will be reflected back from the seafloor will also depend on the frequency, so also the reflection loss is frequency dependent.

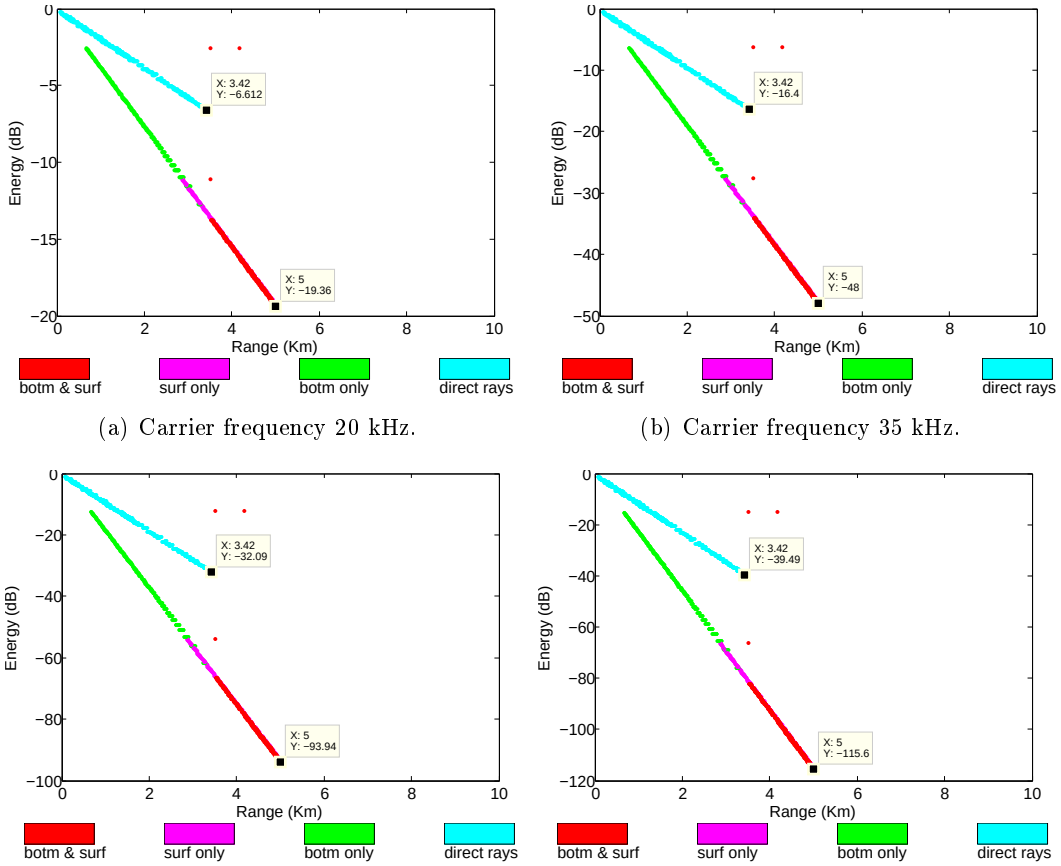

(a) Carrier frequency 20 kHz.

(b) Carrier frequency 35 kHz.

(c) Carrier frequency 60 kHz.

(d) Carrier frequency 75 kHz.

Figure 4.7: Absorption loss for different carrier frequencies. The different colors give loss for direct waves and waves that have been reflected by the bottom and the surface.

In these simulations four different carrier frequencies were tested and compared: 20 kHz, 35 kHz, 60 kHz and 75 kHz. Since the EasyPLR program gives the results of the loss in three categories it is quite easy to analyze how changing the carrier frequency will affect the loss. In this simulation the absorption loss, reflection loss and spreading loss is analyzed. Spreading loss is not frequency dependent and is therefore not interesting in this discussion.

Looking at the absorption loss it is as expected very dependent on the carrier frequency and in figure 4.7 the absorption loss is shown for the four different carrier frequencies. The standard carrier frequency that is being used in this study is 35 kHz and for direct waves the maximum energy loss is -16.4 dB at 3.42 km. For lower frequencies it should be expected that there is lower absorption loss than at 35 kHz. And at 20 kHz this expectation is confirmed, with an energy loss of -6.6 dB at the same distance. The difference in energy loss is 9.8 dB between 20 kHz and 35 kHz, which is substantial. Also for the bottom reflected waves, surface reflected waves and waves both surface and bottom reflections the loss is increasing with distance, and is higher at

35 kHz than 20 kHz. The maximum loss at 5 km is -19.36 dB for 20 kHz and -48 dB for 35 kHz for waves with multiple reflections. This is a difference of 28.64 dB, which is substantial higher than the difference for the direct waves at 3.42 km.

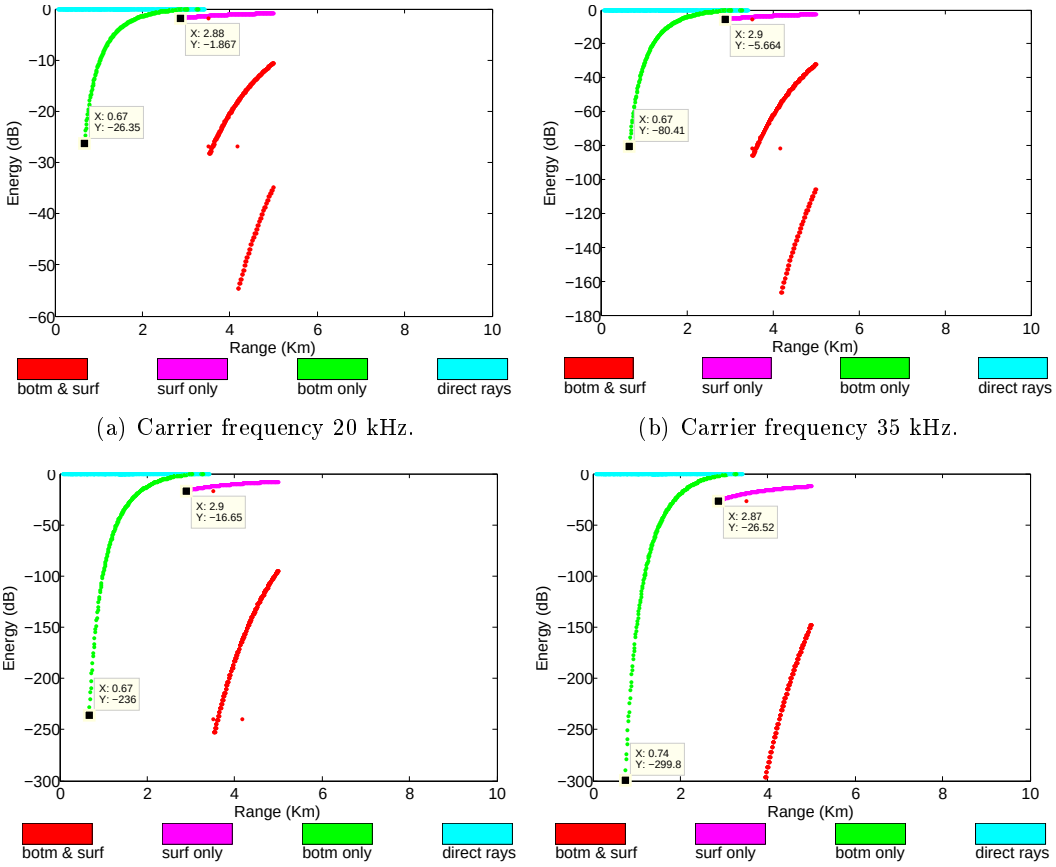

(a) Carrier frequency 20 kHz.

(b) Carrier frequency 35 kHz.

(c) Carrier frequency 60 kHz.

(d) Carrier frequency 75 kHz.

Figure 4.8: Reflection loss for different carrier frequencies. The different colors give loss for direct waves and waves that have been reflected by the bottom and the surface.

By increasing the carrier frequency to 60 kHz and 75 kHz the absorption loss is increased compared to the two lower carrier frequencies. At 60 kHz the maximum loss at 3.42 km for the direct waves are -32.09 dB and for 75 km -39.49 dB, a difference of 7.4 dB. This means that the difference is smaller between 60 kHz and 75 kHz than for 20 kHz and 35 kHz. Going from 20 kHz to 75 kHz will for the direct waves give an increase in the loss of totally 32.88 dB, and this is a quite large difference. For waves with multiple reflections with a receiver at 5 km the loss is -93.94 dB for 60 kHz and 115.6 dB for 75 kHz. At 5 km for waves with multiple reflections the difference in loss between 20 kHz and 75 kHz is 96.24 dB, which is extremely high.

The reflection loss will not have the same linear logarithmic behavior for increasing distance because in it depends a lot on the incoming angle. In general there is a huge difference between loss in the seafloor and loss in the surface. At the surface there will be very little loss compared to the seafloor and this can be seen in figure 4.8 where the reflection loss is shown for different frequencies. There is a major difference in the reflection loss between the different frequencies, as it is for the absorption loss. But the shape of the curves for the reflection loss is the same for

all the four frequencies. The most characteristic with the reflection loss is that for the bottom reflected waves the loss is decreased for greater distance. This is most likely caused by the change in the incoming angle of the waves hitting the seafloor. This can be seen in figure 4.3 where waves hitting the seafloor have a larger incoming angle for shorter distances than for longer distances.

As mentioned the reflection loss is largest for bottom reflected waves at short distances and the loss will depend severely on the carrier frequency. For a carrier frequency of 20 kHz the maximum loss for bottom reflected waves will be -26.35 dB and for 35 kHz the reflection loss will be -80.41 dB, both at a distance of 0.67 km. This gives a difference in the reflection loss of 54.06 dB, which is much higher than the difference in the absorption loss for the direct waves. For carrier frequencies of 60 kHz and 75 kHz the bottom reflected waves have even a higher reflection loss with -236 dB and -299.8 dB respectively.

For the surface reflected waves the reflection loss is much lower and at 20 kHz the reflection loss has a maximum of -1.867 dB and for 35 kHz the reflection loss is -5.664 dB. This is quite low, but for 60 kHz and 75 kHz the surface reflected waves have substantially higher reflection loss. At 60 kHz the reflection loss is -16.65 dB and at 75 kHz the reflection loss is -26.52 dB. This shows that the reflection loss is severely dependent on the frequencies and needs to be taken into account when choosing the carrier frequency.

It should be mentioned that loss in general is not necessarily a negative thing. For the direct waves the loss is a problem since it reduces the energy and thereby causes problem in detecting the signal. But for the other multipath such as bottom reflected waves, surface reflected waves and waves that are reflected in both surface and bottom it might be advantage with high loss. In the receiver these multipath may give disturbance to the received signal from the direct wave. But since the multipath have experienced a much higher loss than the direct waves the multipath may be so weak that they will not affect the data transmission substantially. And this is a huge advantageous. This can be seen in figure 4.4(b) where time-delay is shown, and the bottom reflected wave (green) is much weaker than the direct wave (light blue). The dotted line in the plot shows the 10 db limit, meaning how large a signal needs to be to have an amplitude value that is 10 dB lower than the largest signal. There will be very little disturbance in a transmission if there is a difference between a multipath and a direct wave of more than 10 dB.

It is clear that having a very high carrier frequency such as 75 kHz will give a very high loss but with the possibility of having very high data rate if the signal is not disturbed through the transmission. The advantage of having a lower carrier frequency is that the loss is reduced, but with lower possible data rate. In general how high loss that can be accepted in an underwater acoustic sensor network will depend on the hardware system and the hydrophones in the receiver. Too high loss will give a too weak signal so the receiver will not be able to detect the signal. This can be solved by increasing the transmission energy, but at the cost of higher energy consumption.

4.4 Different sound speed profiles

In the simulations done in the EasyPLR program Quadrature Phase Shift keying (QPSK) was chosen to be used at the modulation technique. The reason for this was based on the advantages

compared to binary shift keying mentioned in section 3.1.2 and that is not too complicated to implement in Matlab.

The simulation was performed by sending a modulated signal through EasyPLR and then adding Additive white Gaussian noise (AWGN) to the signal to simulate noise. Four different sound speed profiles were chosen to be used in the simulations done in EasyPLR. These sound speed profiles are given in figure 4.9 and are labeled in this study as case 1, 2, 3 and 4. For more details about the sound speed profiles see table A.1 Appendix A.

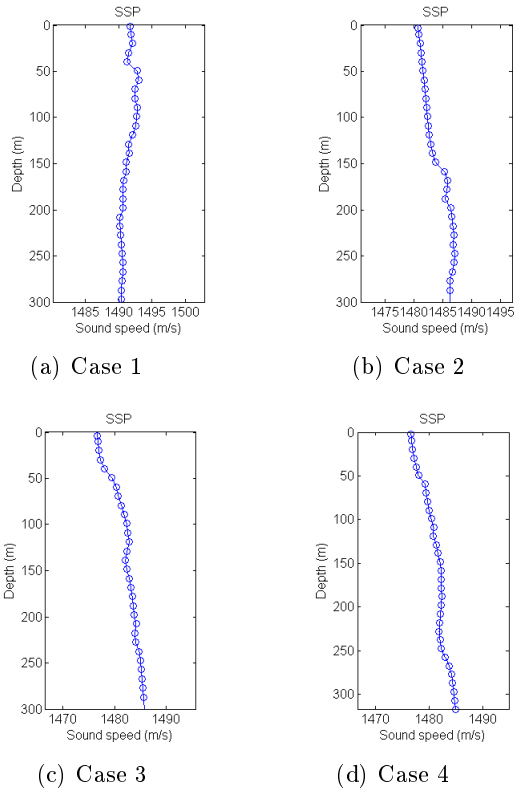

(a) Case 1 (b) Case 2

(c) Case 3 (d) Case 4

Figure 4.9: Different sound speed profiles, for details about the sound speed profiles see table A.1 appendix A.

In the simulations of QPSK modulation technique different level of noise was added to see how this would affect the different sound speed profile cases. Case 1 was used as a reference when calculating the Signal-to-noise ratio (SNR) for the four different cases. The transmitter was placed at horizontal distance of 0 m and the receivers were placed at 1 km, 2 km and 3 km at a depth of 250 m with the seafloor at 300 m.

In figure 4.13 the received message points are shown for the four different cases. Case 1 has a SNR value of 14 dB, which is the best result for the four cases, and compared to case 2 has a SNR value of 5 dB that is substantially lower than case 1. Case 2 has a bit error ratio (BER) of 0.0554 while case 1 has a BER almost equal to zero. This result is not surprising consider the received pulse in case 2 that has a much lower amplitude value compared to the other cases. This can easily be seen in figure 4.10(b) where the received pulse for case 2 is shown. Looking at case 3 and 4 in figure 4.13 case 3 three has a SNR value of 11 dB while case four has a SNR

value of 12 dB. Normally it should be expected that case 4 will have a better performance than case 3, but looking at the message points case 3 actually has a greater distance from the message points to the symbol boundaries than case 4 has. This means that the chance of errors is greater for case 4 than case 3 even with lower SNR value. And the bit error ratio (BER) for case 3 is $1.25 \cdot 10^{-5}$ while for case 4 the BER is 0.012. This result may be caused by the difference in the received pulse shapes. In figure 4.10 the four received pulses is shown and the clear difference between the two pulse shapes in case 3 and 4 is that case 4 has more of the pulse values divided between positive and negative values. Since QPSK demodulator uses integration to detect the phase values this will affect the result. And the detector is optimized for raised cosine pulses that will have most of its signal points as either positive or negative values depending on the transmitted symbol.

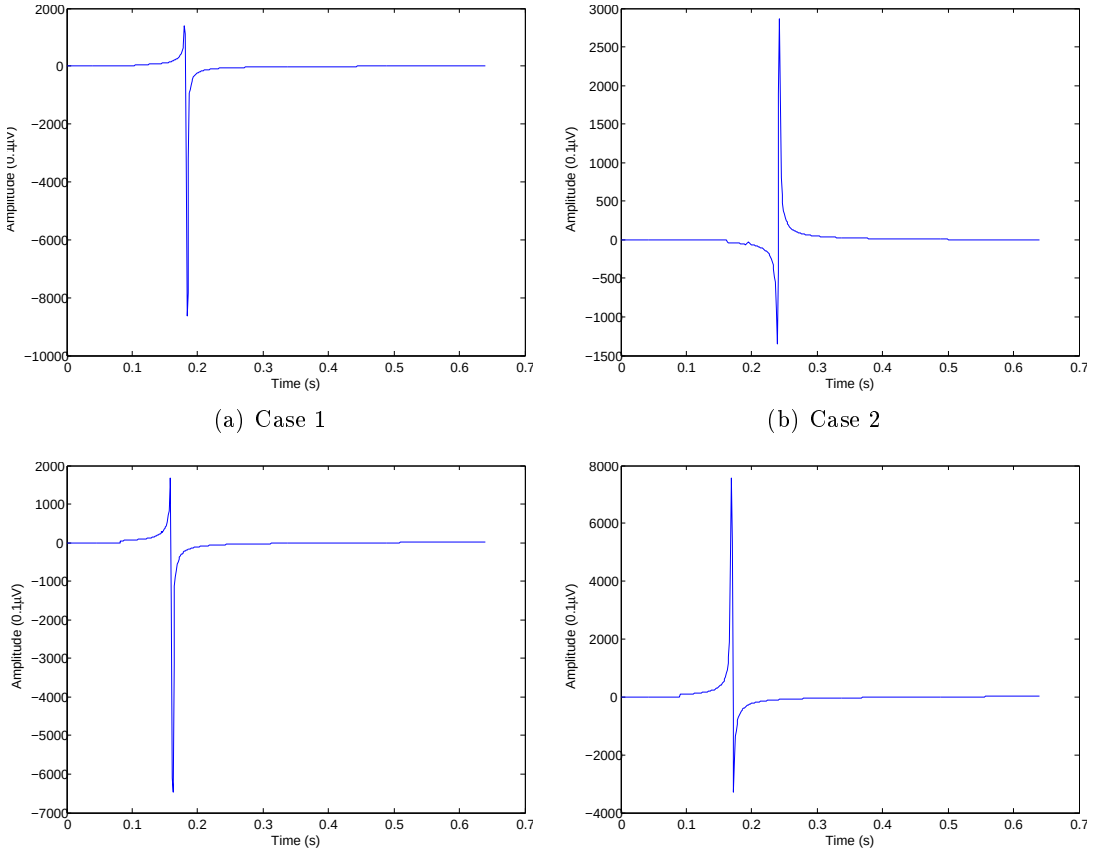

(a) Case 1

(b) Case 2

(c) Case 3

(d) Case 4

Figure 4.10: Received pulses at 1000 m for different sound speed profiles given in figure 4.9

By reducing the noise level the SNR value is increased, and for case 1 the SNR value is increased to 20 dB. By using the same noise level for the four cases different result is experienced as shown in figure 4.14. The major difference by increasing the SNR value is that the detection points have less spreading since the noise level has been reduced. Just as in figure 4.13 where the SNR value was lower it is case 1 that has the greatest distance to the symbol boundaries. As can be seen in figure 4.14 it is case 2 that has the worst performance, while case 3 has better performance than case 4 even though the SNR value is 1 dB lower. For case 2 the reduction

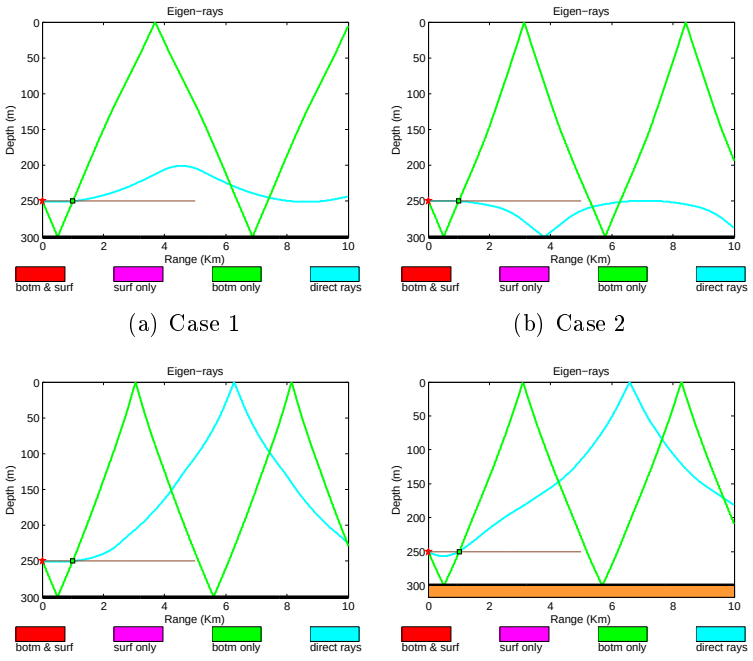

(a) Case 1 (b) Case 2

(c) Case 3 (d) Case 4

Figure 4.11: Eigen-rays at 1000 m for different sound speed profiles given in figure 4.9

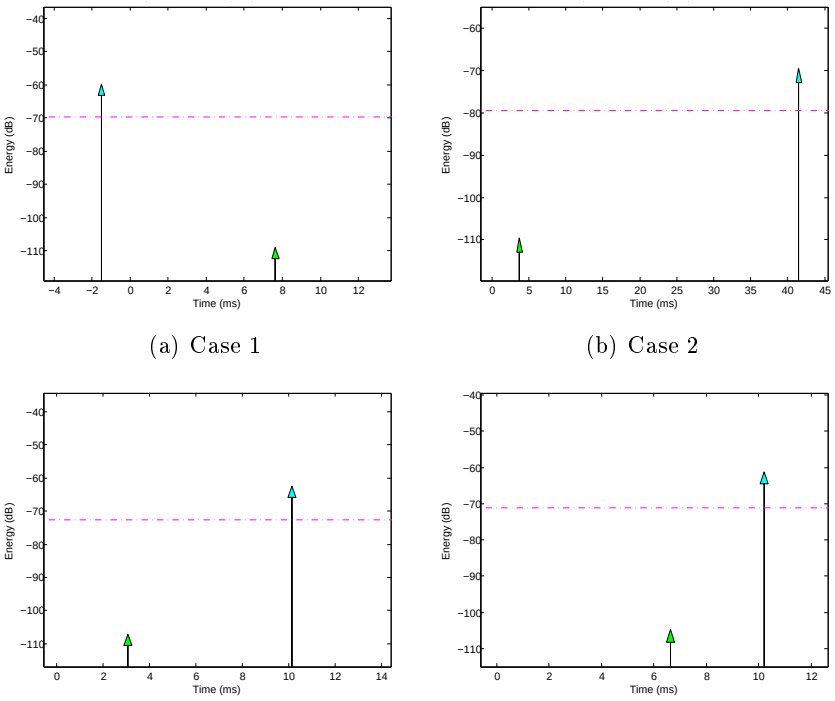

(a) Case 1 (b) Case 2

(c) Case 3 (d) Case 4

Figure 4.12: Time-delay at 1000 m for different sound speed profiles given in figure 4.9.

of the noise level has increased the SNR value from 5 dB to 9.5 dB, and thereby reducing the chance of errors greatly.

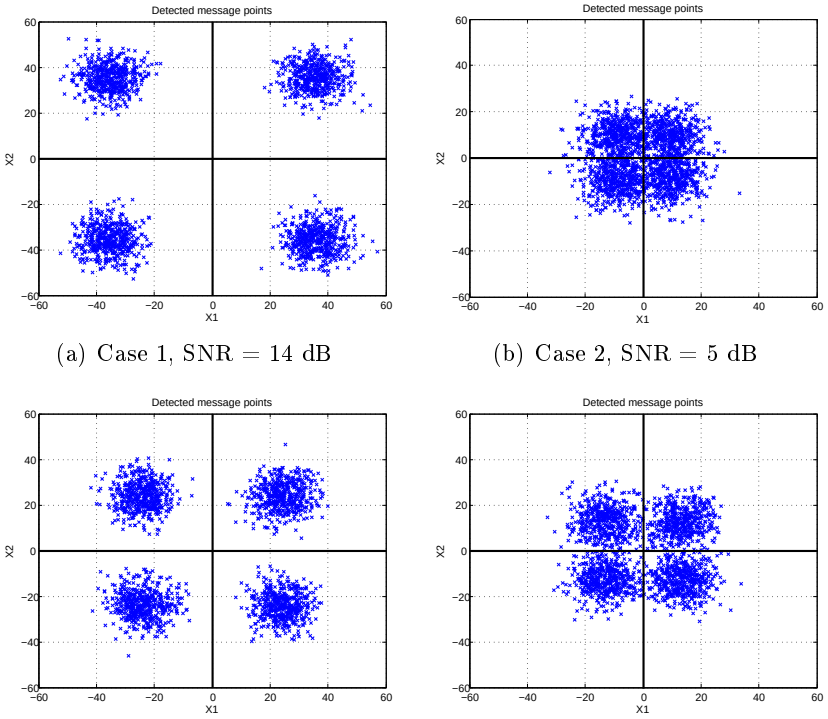

(a) Case 1, SNR = 14 dB

(b) Case 2, SNR = 5 dB

(c) Case 3, SNR = 11

(d) Case 4, SNR = 12 dB

Figure 4.13: Calculated message points at 1000 m for different sound speed profiles given in figure 4.9.

The variation in the received pulses is caused by the different sound speed profiles. Since the different cases have different sound speed profiles the propagation of the rays will be different in all cases and at the receiver the signal will consist of both direct waves and reflected waves. For a better understanding figure 4.11 show the eigen-rays for the four cases. In the figures the receiver at 1000 m is indicated with a green mark, and the blue line indicates direct waves and the green line indicates the reflected waves from the seafloor. These eigen-ray plots shows that in all four cases the received pulses will consist of both direct waves and bottom reflected waves. The question is how this will affect the results since the eigen-ray plots do not give any indication on the energy difference between the multipaths and the time-spread between the different rays. In figure 4.12 the time-delay for the four different cases is shown. In each plot both the direct ray and the bottom reflected ray is shown with time delay and energy level in decibel. The time delay and time-spread is different for all four cases because of the difference in the sound speed profile. But there is one important similarity between all four cases and that is the large energy difference between the direct rays and the bottom reflected rays. For example in figure 4.12(a) for case 1 there is a energy level difference between the direct wave and the bottom reflected wave of 49.2 dB. This is a very large difference and means that the bottom reflected wave will almost not at all affect the direct wave.

It should be mentioned that the direct waves have experienced a 90° phase shift because the wave is going through a turning point and the detection points have been changed by 90°. This

means that all the detected symbols are wrong, but this can easily be solved by first sending a known test sequence to adjust the detected symbols to the phase shift. In the case of the received pulse only consisting of reflected waves and not a direct wave the same procedure can be performed to adjust the phase shift. How often this test procedure needs to be transmitted will depend on how fast the sound speed profile is changing. As long as the changes in the sound speed profile do not happens too often the test sequence will not reduce the data transmission.

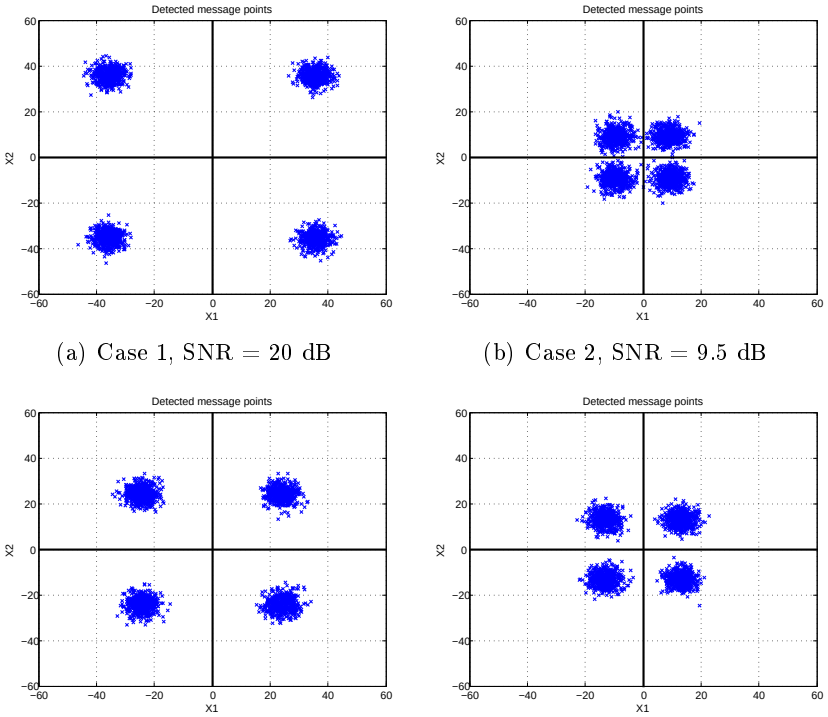

(a) Case 1, SNR = 20 dB

(b) Case 2, SNR = 9.5 dB

(c) Case 3, SNR = 17 dB

(d) Case 4, SNR = 18 dB

Figure 4.14: Calculated message points at 1000 m with reduced noise level for different sound speed profiles given in figure 4.9.

Increasing the transmission distance from 1000 m to 3000 m will increase the loss severely as discussed in section 4.3. In figure 4.15 the received pulses at 3000 m for the different sound speed profiles are shown. The clearest result is that he four different cases have very different pulse shapes, and this is caused by the variation in the sound speed profiles. Just by looking at the pulses it is clear that case 2 will have a bad performance since the pulse shape consist of two waves with almost the same energy level. This can be verified by the eigen-ray plot in figure 4.16(b) and the time delay plot in figure 4.17. As can be seen the received pulse consist of both bottom reflected wave and a surface reflected wave with almost the same energy level, respectively -101.5 dB and -102.8 dB. For case 1 the received pulse in figure 4.15(a) only consist of a bottom reflected wave as can be seen the eigen-ray plot in figure 4.16(a), and this will give a quite weak amplitude and thereby vulnerable to noise disturbance. For case 3 the received pulse in figure 4.15(c) consist of both a direct wave, a bottom reflected wave and a surface reflected wave as seen in the eigen-ray plot in figure 4.16(c) and the time delay plot in figure 4.17(c). But in the time delay plot the direct wave has much higher energy than the multipaths, and only a very little disturbance can be seen in the received pulse in figure 4.15(a). For case 4 the received

pulse consists of a direct wave and a bottom reflected waves, but in the time delay plot in figure 4.17(d) the direct wave has much larger energy than the bottom reflected wave.

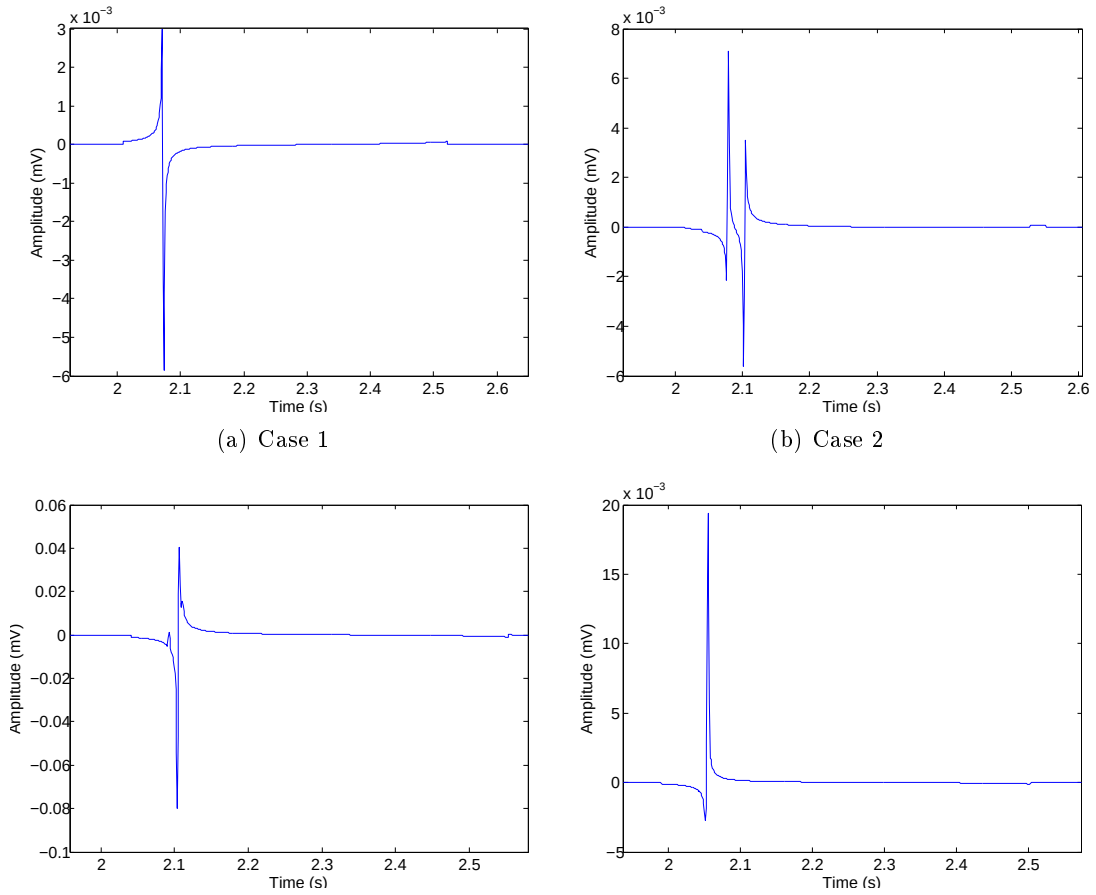

(a) Case 1 (b) Case 2

(c) Case 3 (d) Case 4

Figure 4.15: Received pulses at 3000 m for different sound speed profiles given in figure 4.9

By using the noise level equal to a SNR value of 40 dB for case 1 at 1000 m the message points are calculated for the different cases in figure 4.18 at 3000 m. As expected from the received pulses case 1 and 2 have a very bad performance where the message points are crossing the symbol boundaries and causing symbol errors. This gives a bit error ratio of (BER) 0.242 for case 1 and a BER of 0.236 for case 2. Since case 1 has a very weak received pulse the SNR value is only 1.5 dB while case has a little bit higher with a SNR value of 3.24 dB. For case 3 the SNR value is 17 dB while case 4 has a SNR value of 9 dB. Still looking at the detected message points case 4 actually has a little better performance than case 3. Case 4 has a BER of 0.0051 while case 3 has a BER of 0.0213. This may caused by the fact that the received pulse shape in case 3 is affected by several multipaths and that pulse consist of a large part of positive values and an even larger part of negative values. As previous mentioned this will affect the result in the receiver since it uses an integrator in the receiver. For case 4 almost all of the pulse values are positive giving a good detection result. By increasing the SNR values and using the noise level equal to a SNR value of 60 dB for case 1 at 1000 m the result becomes much better. As seen in figure 4.18 case 1 and 2 have now much better performance and there is some distance to the

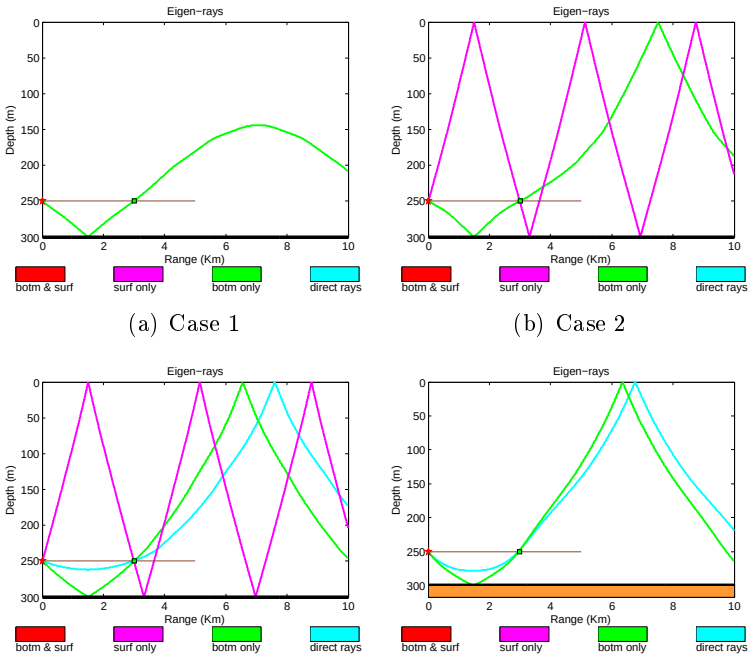

(a) Case 1 (b) Case 2

(c) Case 3 (d) Case 4

Figure 4.16: Eigen-rays at 3000 m for different sound speed profiles given in figure 4.9

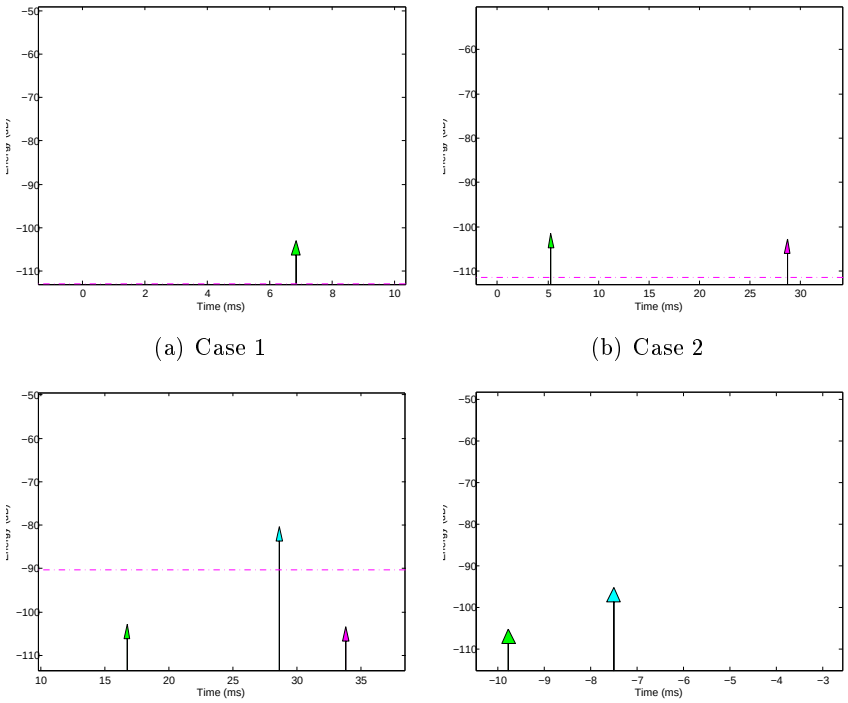

(a) Case 1 (b) Case 2

(c) Case 3 (d) Case 4

Figure 4.17: Time-delay at 3000 m for different sound speed profiles given in figure 4.9.

detection boundaries. Case 1 has a SNR of 16 dB while case has a SNR value of 20 dB. The two cases are now much more robust against noise, but compared to case 3 and 4 they have still quite bad performance. For case 3 and 4 the distance from the detection points to the symbol boundaries are quite large and the chance of getting symbol errors is very little for this noise level.

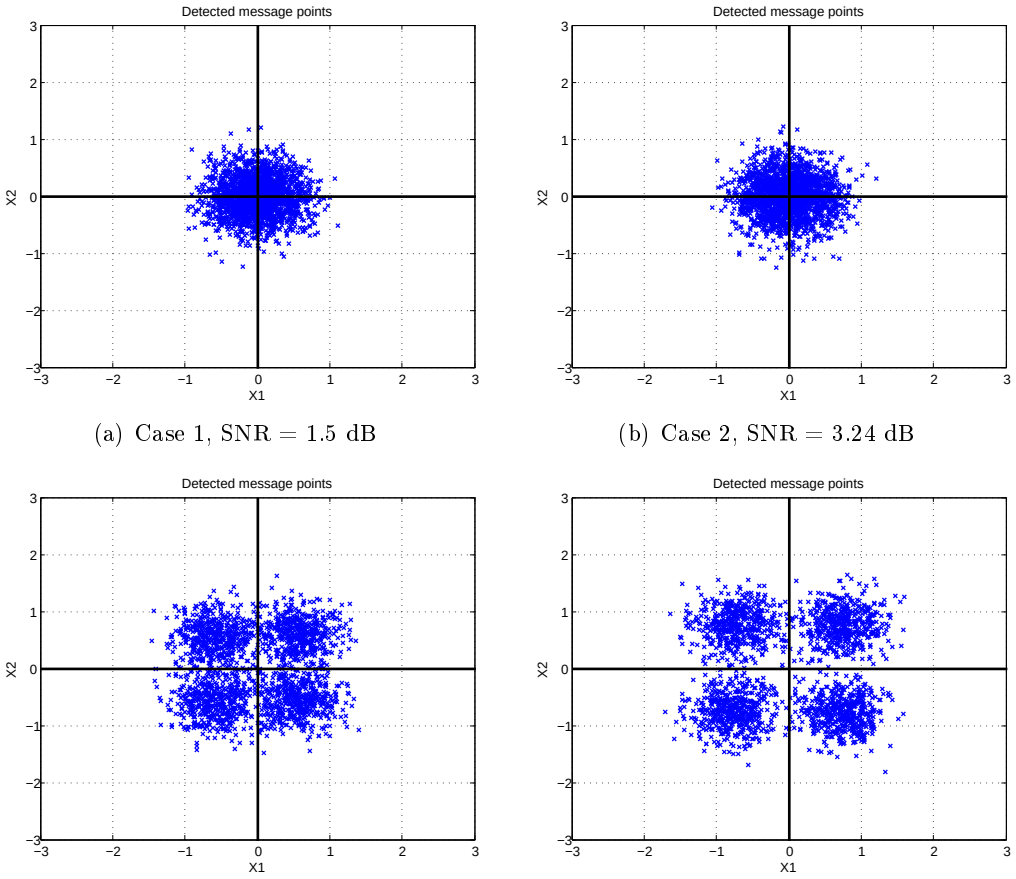

(a) Case 1, SNR = 1.5 dB

(b) Case 2, SNR = 3.24 dB

(c) Case 3, SNR = 17 dB

(d) Case 4, SNR = 9 dB

Figure 4.18: Calculated message points for different sound speed profiles, given in figure 4.9, at 3000 m with the same noise level as case 1 had at 1000 m for SNR equal to 40 dB.

In general these simulation results show that there is substantial difference in the performance depending on the given sound speed profiles. This means that the possible data rate for a given energy level will vary with both time and place. For a wanted data transmission-rate the transmitter may need to transmit at a high energy-level to deal with local factors affecting the data transmission. For shorter distances such as 1 km this study shows that normally direct waves will be received and the energy level between these and the multipaths will be so large that the multipaths will have very little influence on the received data transmission.

But for greater distances such as 3 km the picture become a little bit more complex. In situations where direct waves are being received the energy levels between the direct waves and the multipaths will be so large that the multipaths will only affect the data transmission in some degree. The multipaths will have a higher influence at 3 km than at 1 km but this is still not a

major problem as seen in the simulations. But in situations where no direct waves are received and only bottom reflected waves and surface reflected waves are received the performance is much worse. This is because the multipaths will in general have a higher loss because of longer travelling distance and reflection loss. Since the signals are much weaker they are more vulnerable to noise disturbance. Another problem that has been shown in this study is situations where different multipaths have almost the same energy level. If the time-spread between the multipaths is not too large the received pulse will consist of several waves and this will give disturbance to the received data. To summarize for short distances such as 1 km multipaths will be a very little problem but at larger distances such as 3 km multipaths may be a problem in some situations.

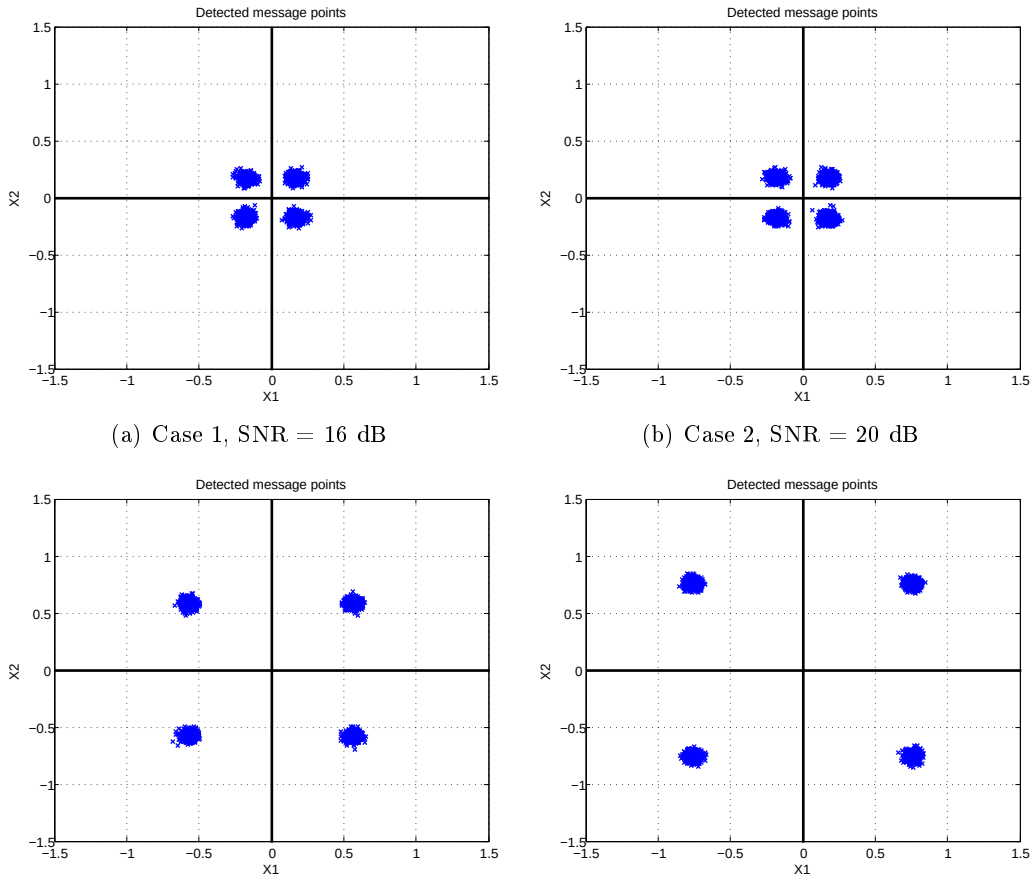

(a) Case 1, SNR = 16 dB

(b) Case 2, SNR = 20 dB

(c) Case 3, SNR = 37 dB

(d) Case 4, SNR = 26 dB

Figure 4.19: Calculated message points for different sound speed profiles, given in figure 4.9, at 3000 m with the same noise level as case 1 had 1000 m for SNR equal to 60 dB.

4.5 Direct sequence spread spectrum

The final simulations that were performed were to simulate direct sequence spread spectrum (DSSS). To simulate direct sequence spread spectrum (DSSS) the EasyPLR program had to be additional modified to deal with the spreading codes. To generate the spreading codes a Gold

code generator in Simulink in Matlab was used. The Gold code generator in Simulink is quite easy to use as long as the correct set of preferred pairs are being used, as described in section 3.4.

One important difference when using spreading codes is that the transmitted pulse may get an increased bandwidth. This is caused by the fact that the pulse shape is changed because of multiplication with a spreading code and thereby increasing the bandwidth. Several of the received pulses in the direct sequence spread spectrum simulations got large oscillations on the signal. This effect may be caused by the so called Gibbs phenomenon and the solution is to increase the bandwidth. When the bandwidth was increased in the simulations the oscillation effect was substantially reduced.

As mentioned in the section 3.3 there are several spreading techniques that can be used in CDMA. But as discussed directs sequence spread spectrum (DSSS) has the best performance and is therefore chosen as the spreading technique for the simulations in this study. In figures 3.7 and 3.8 in section 3.3 the transmitter and receiver is shown for a general DSSSS system. But depending on the modulation method the design will vary to some degree. In the simulation Quadratue phase shift keying (QPSK) in combination with Binary phase shift keying (BPSK) is used.

4.5.1 Binary phase shift keying Direct sequence spread spectrum

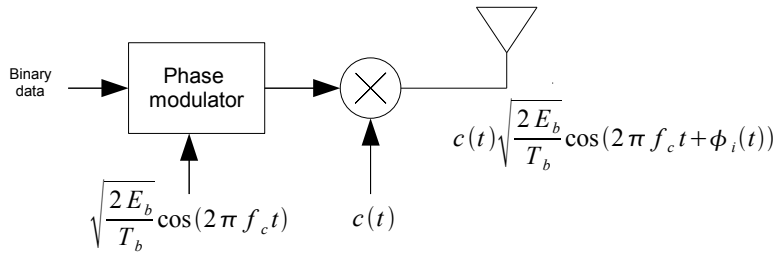

Figure 4.20: BPSK Direct sequence spread spectrum transmitter

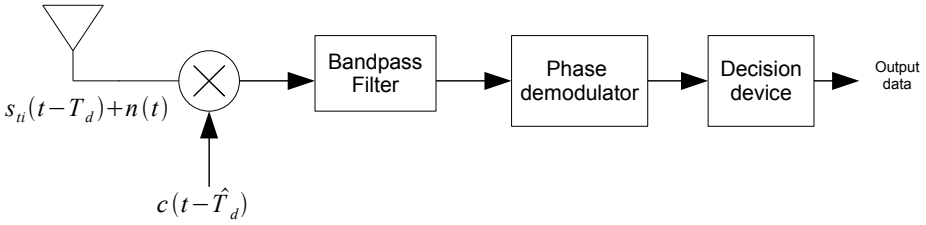

Figure 4.21: BPSK Direct sequence spread spectrum receiver

How the direct-sequence spread spectrum system is designed depends on the modulation technique. The simplest form is to use binary phase shift keying (BPSK), [18]. As described in section 3.1.1 the BPSK will modulate the signal with 180° phase shift as seen in equation 4.1.

$$s_i(t) = \sqrt{\frac{2E_b}{T_b}}\cos(2\pi f_c t + \theta_i(t)), \qquad i = 1, 2 \tag{4.1}$$

The modulated signal $s_i(t)$ will in DSSS be multiplied with the spreading code c(t), as showed in figure 4.20. The transmitted DSSS signal will then be:

$$s_{ti}(t) = c(t)\sqrt{\frac{2E_b}{T_b}}\cos(2\pi f_c t + \theta_i(t)), \qquad i = 1, 2 \tag{4.2}$$

This signal will then be transmitted through the underwater acoustic channel. The transmitted signal will experience time delay through the channel, and also phase displacement. Some noise may also disturb the signal. In the receiver seen in figure 4.21 the received signal will be despread through a multiplication with the same spreading code as in the transmitter. The signal component will after the depsreading mixer be:

$$s_{ds}(t) = c(t - \hat{T}_d)c(t - T_d)\sqrt{\frac{2E_b}{T_b}}\cos(2\pi f_c t + \theta_i(t) + \phi) + n, \qquad i = 1, 2 \tag{4.3}$$

Here T_d is the actual time delay and $\hat{T}_d$ is an estimate of the time delay. As seen in figure 4.20 the transmitted signal will be multiplied with the spreading code $c(t - \hat{T}_d)$. If the estimate of the time delay is equal to the actual time delay the received despread signal will be the same as the generated signal before spreading, except from the changes caused by noise and phase displacement. The reason for that the depsreading should give the same result as the generated signal is that:

$$c(t - T_d)c(t - \hat{T}_d) = 1 \qquad if; \;\; T_d = \hat{T}_d \tag{4.4}$$

since $1 \times 1 = 1$ and $(-1) \times (-1) = 1$. After the despreading the signal will work as a regular binary phase shift keying signal.

4.5.2 Quadrature phase shift keying Direct sequence spread spectrum

As discussed in section 3.1.2 the use of Quadrature-shift keying (QPSK) is more effective than BPSK since it is able to send two bits instead of one bit. And in this simulation QPSK direct sequence spread spectrum (DSSS) is used. The configuration for the direct sequence spread spectrum system (DSSS) that is used is the so called *dual-channel QPSK* that is shown in figure 4.22 from [18]. The principle is to use BPSK data modulators in the in-phase and quadrature-phase QPSK channels. Each of the channels will have different BPSK data modulators and will generate positive and negative pulses. As can be seen in figure 4.22 these two components are each multiplied with different spreading codes, $c_1(t)$ and $c_2(t)$. The sine component is multiplied with $-c_2(t)$ to get the correct sum in equation 4.5. Then the two signals are added together and this gives the following result:

$$s_i(t) = \sqrt{\frac{E}{T}}d_1(t)c_1(t)\cos(2\pi f_c t) - \sqrt{\frac{E}{T}}d_2(t)c_2(t)\sin(2\pi f_c t) \tag{4.5}$$

where $d_1(t)$ and $d_2(t)$ are the respectively BPSK modulated data signals that are inputs to the QPSK DSSS transmitter.

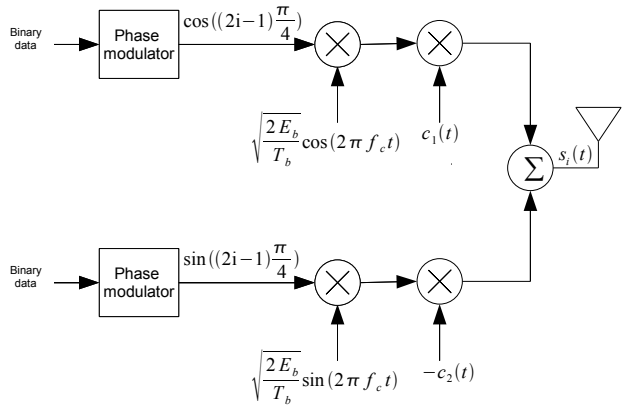

Figure 4.22: QPSK Direct sequence spread spectrum transmitter

In the receiver that is shown in figure 4.23 the signal is first divides into two separate receivers where the received signal is multiplied respectively with the spreading codes $c_1(t - \hat{T}_d)$ and $c_2(t - \hat{T}_d)$, that is the original spreading codes with time delay. Then the received signal is also multiplied with either sine or cosine carrier wave, and finally binary phase shift keying demodulating is used to detect the two signal channels. The advantage of this system is that the detection can be performed by a simple binary phase shift keying (BPSK) demodulator for each channel.

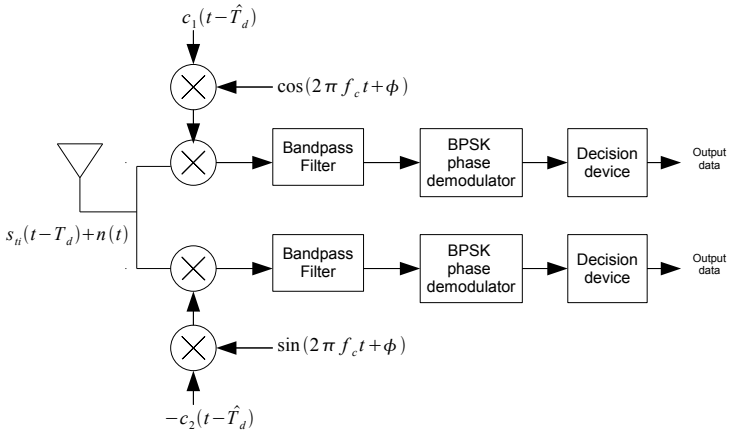

Figure 4.23: QPSK Direct sequence spread spectrum receiver

4.5.3 Results

In the simualtions of Quadrature phase shift keying (QPSK) with Direct sequence spread spectrum (DSSS) noise was added to the signal in the same way as in the previous section with

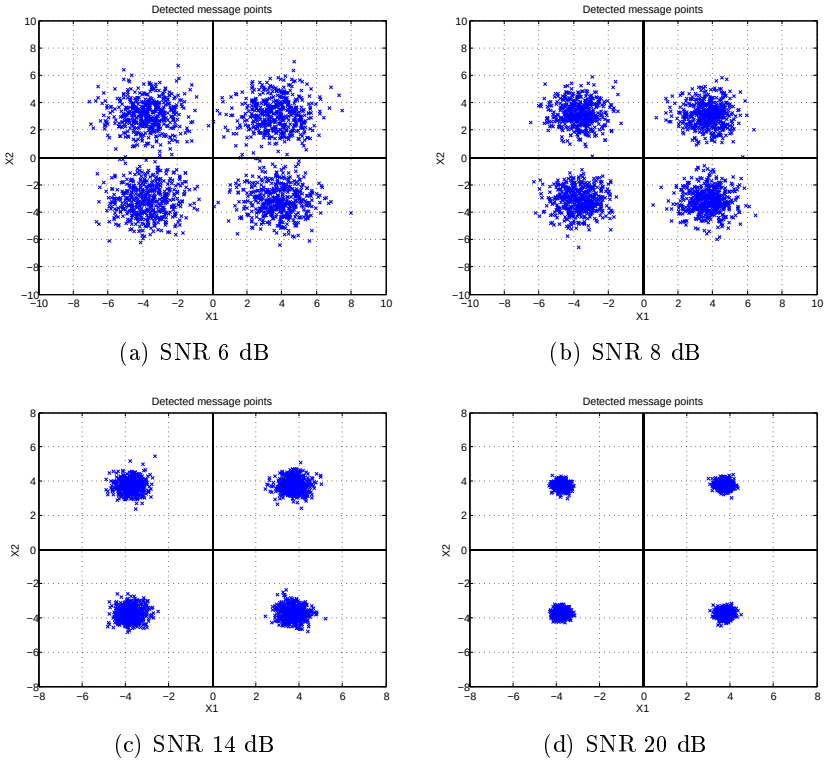

(a) SNR 6 dB (b) SNR 8 dB

(c) SNR 14 dB (d) SNR 20 dB

Figure 4.24: Calculated message points for different SNR values at 1000 m.

the received pulse at 1000 m as the noise reference. To show the received results after demodulation the in-phase and the quafrature channel is plotted together in the same way as regular quadrature phase shift keying (QPSK).

In figure 4.24 the received demodulated signals at 1000 m are shown with different Signal-to-noise ratio levels. For a Signal-to-noise ratio (SNR) level of 6 dB (figure 4.24(a)) and 8 dB (figure 4.24(b)) the signal space plot shows that the received detection point varies a lot and the detection points are very close boundary of other symbols. So the chance of getting symbol errors is quite high. In figure 4.24(c) and 4.24(d) the SNR values are increased to 14 dB and 20 dB respectively. It can easily be seen that the variation in the detection points now are much lower and that the distance from the the detection points to the boundary for other symbols are greater. The interesting result is that going from a SNR value 14 dB to a SNR value of 20 dB does not increase the performance substantially. The detection point for 20 dB have of course less variation than for 14 dB and the distance to the boundary for other symbols are larger than for 14 dB, but the difference is not that huge. In wireless communication there will always be a tradeoff between having few symbol errors and reducing the power consumption. The advantage of transmitting at 14 dB compared to 20 dB is reduced power consumption, but with the cost of higher probability of symbol errors. In real applications a power consumption analysis can be useful way to decide what SNR value the transmission system should use.

Having the receiver at 3000 m instead of 1000 m is a major difference because of high loss in underwater acoustic communication as shown in section 4.3. In figure 4.25 the signal space for detected message points is shown for different SNR values. In parenthesis the SNR value for

the same noise level at 1000 m is also given. Going from 1000 m to 3000 m with the same noise level will give a reduction of SNR value from 14 dB to 1 dB. This is of course a very high reduction and as can be seen in figure 4.25(a) the variation in the detection points are quite large and causes symbols errors. Increasing the SNR value to 3 dB will reduce the large variation in detection points, but will still be quite high, as can be seen in figure 4.25(b). A SNR value of 3 dB will have the same noise level as a SNR value of 20 dB at 1000 m. Even though there is less variation in the signal detection points symbol errors still occurs because the detection points is crossing the symbol boundaries. The simplest way to reduce the symbol errors is to increase the SNR value and in figure 4.25(c) the SNR value is increased to 20 dB and it shows that the performance in substantially improved. The variation in the detection points is now very little and the distance to the symbol boundaries is much larger. And by increasing the SNR value to 60 dB the variation in detection points is even smaller. But compared to transmitting at 1000 m the performance is not that good. And for both SNR values of 20 dB and 40 dB at 3000 m will need transmission energy that will give SNR values of 40 dB and 60 dB respectively at 1000 m.

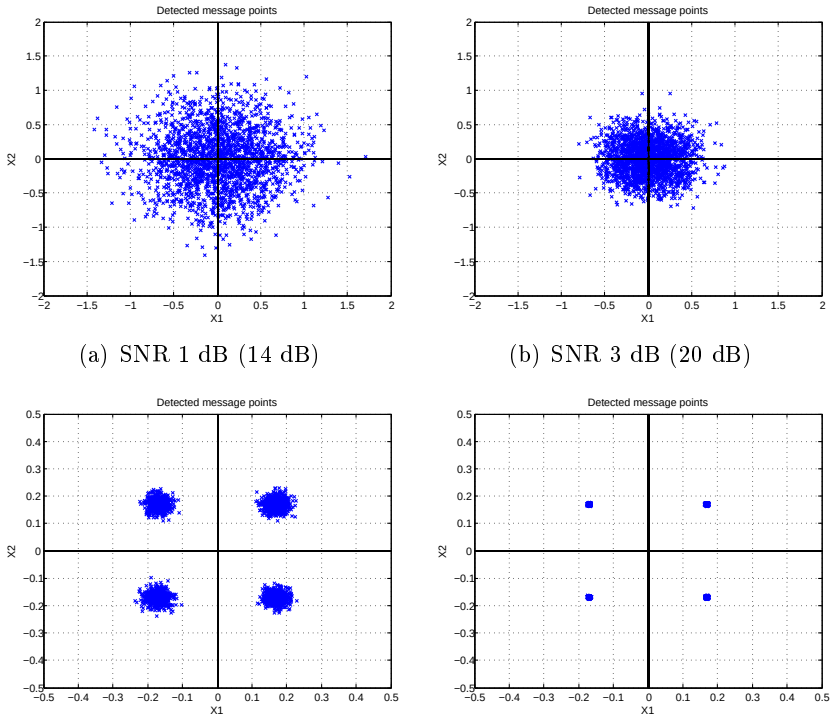

(a) SNR 1 dB (14 dB)

(b) SNR 3 dB (20 dB)

(c) SNR 20 dB (40 dB)

(d) SNR 40 dB (60 dB)

Figure 4.25: Calculated message points for different SNR values at 3000 m with the SNR value at 1000 m in parenthesis for the same noise level.

The advantages of direct sequence spread spectrum (DSSS) that are mentioned in section 3.3 are good arguments for using DSSS in underwater acoustic sensor networks and the performance in the simulations in this study are quite good and with some optimization the results can be better. The challenge in DSSS is to have good time synchronization between the transmitted code spreader and the received code despreader. To reduce the problem of noise better filters can be used in the receiver. The disadvantage with using spreading codes is that the bandwidth is

increased and this can be a problem in band-limited situations. To deal with multiple users and noise the direct sequence spread spectrum has been used with Gold codes as spreading codes. These spreading codes have worked for detecting the correct symbols.

Chapter 5

Conclusion

In this study underwater acoustic communication has been simulated by using the EasyPLR program in Matlab. Different types of pulse-shapes have been tested with the same performance except for the frequency response. In simulation of underwater acoustic communication different carrier-frequencies have been tested. When choosing the carrier frequency there will be a tradeoff between having high frequency to get high data rates and minimizing the loss. Lower carrier frequency will reduce the loss but at the cost of lower data rates. Since both the absorption loss and the reflection loss depends heavily on the frequency there is no clear answer to what carrier frequency that should be used. But by using EasyPLR it can be quite easy to model the loss for different carrier frequencies and thereby deciding how high carrier frequency the system can have and still have acceptable loss. To use Quadrature phase shift keying as the modulation technique works very good, but with varying result the depending on the sound speed profile. In general these simulation results show that there is substantial difference in the performance results depending on the given sound speed profiles because of different multipath and refraction effects. This means that the possible data rate for a given energy level will vary with both time and place. For a wanted data transmission-rate the transmitter may need to transmit at a high energy-level to deal with local factors affecting the data transmission. For shorter distances such as 1 km this study shows that normally the direct waves will be received and the energy level between these and the multipaths will be so large that the multipaths will have very little influence on the received data transmission. The reflection loss is actually an advantage to reducing the multipaths. But for longer distances such as 3 km the multipath will have a higher influence on the communication. In situation where no direct waves are received only multipaths waves will be detected and they are much weaker and more vulnerable to noise.

To deal with multiple users and noise Direct sequence spread spectrum (DSSS) has been used with Gold codes as spreading codes. The performance of Direct sequence spread spectrum (DSSS) is quite good and by optimizing the system better performance can be achieved. To reduce the problem of noise better filters can be used in the receiver. To detect the correct symbols the spreading codes used in the simulations have worked fine. The challenge in DSSS is to have good time synchronization between the spreading code in the transmitter and the spreading code in the receiver. This is especially challenging in a time variant system.

Turning-point may give a 90 ° phase shift to the received symbols. This can easily be solved by sending a known sequence through the system and thereby adjusting the received phase symbols.

But to make this work it is important that the channel does not change too often so that it reduces the transmission capacity because the known sequence needs to be transmitted often.

To use the EasyPLR program for simulations of underwater communication has worked well. Even though there were some setbacks because of errors in the EasyPLR program they have been corrected and the program is today a good tool for modeling underwater communication. To deal with different types of pulse shapes and modulated signals this program needed to be modified, and for further version of the EasyPLR program it would be an advantage if it supported different types of pulses and also the possibly to modulate the signal.

For further research it would be very interesting to look into communication with multiple users to see how they are interfering with each other and how this would affect the simulation results. In this study additive white Gaussian noise has been used to simulate the noise affecting the communication. It would be interesting to look into other types of noise that would affect the communication and especially noise generated by human activity especially noise from ships. In this study the hardware implementation has not be looked into and this should be done to see how it would be possible to reduce the size of the hardware design and how to minimize the energy consumption for the hardware system.

Bibliography

[1] Ian F. Akyildiz, Dario Pompili, and Tommaso Melodia. Challenges for efficient communication in underwater acoustic sensor networks. *SIGBED Rev.*, 1(2):3–8, 2004.

[2] Ian F. Akyildiz, Dario Pompili, and Tommaso Melodia. Underwater acoustic sensor networks: research challenges. *Ad Hoc Networks*, 3(3):257 – 279, 2005.

[3] Ian F. Akyildiz, Dario Pompili, and Tommaso Melodia. State of the art in protocol research for underwater acoustic sensor networks. *SIGMOBILE Mob. Comput. Commun. Rev.*, 11(4):11–22, 2007.

[4] John R. Barry, Edward A. Lee, and David G. Messerschmitt. *Digital Communication: Third Edition.* Springer, September 2003.

[5] J.A. Catipovic. Performance limitations in underwater acoustic telemetry. *Oceanic Engineering, IEEE Journal of*, 15(3):205–216, Jul 1990.

[6] Mandar Chitre, Shiraz Shahabudeen, Lee Freitag, and Milica Stojanovic. Recent advances in underwater acoustic communications and networking. *IEEE/MTS OCEANS'08 - Canada,*, 2008.

[7] Thomas M. Cover and Joy A. Thomas. *Elements of Information Theory 2nd Edition.* Wiley-Interscience, 2006.

[8] R. E. Francois and G.R. Garrison. Sound absorption based on ocean measurements. part i: Pure water and magnesium sulphate contributions. *J.Acoust. Soc. Am.*, 72(3):896–907, 1982.

[9] R. E. Francois and G.R. Garrison. Sound absorption based on ocean measurements. part ii: Boric acid contribution and equation for total absorption. *J.Acoust. Soc. Am.*, 72(6):1879–1890, 1982.

[10] L. Freitag, M. Stojanovic, S. Singh, and M. Johnson. Analysis of channel effects on direct-sequence and frequency-hopped spread-spectrum acoustic communication. *Oceanic Engineering, IEEE Journal of*, 26(4):586–593, Oct 2001.

[11] Andrea Goldsmith. *Wireless Communications.* Cambridge University Press, New York, NY, USA, 2005.

[12] V.A. Del Grosso. New equations for the speed of sound in natural waters (with comparison to other equations). *J.Acoust. Soc. Am.*, 93(4):1084–1091, 1974.

[13] Simon Haykin. *Communications Systems*. Wiley, 4th edition, May 2000.

[14] Jens M. Hovem. *Marine Acoustics The physics of sound in underwater enviroments*. Norwegian University of Science and Technology, Trondheim, 2008.

[15] Jens M. Hovem and Hefeng Dong. Planeray: An underwater acoustic propagation model using ray tracing and plane wave reflection coefficients. *The Journal of the Acoustical Society of America*, 120(5):3221–3221, 2006.

[16] Jens M. Hovem, Shefeng Yan, Xueshan Bao, and Hefeng Dong. Modeling underwater communication links. *Sensor Technologies and Applications, 2008. SENSORCOMM08. Second International Conference on*, pages 679–686, 2008.

[17] D.B. Kilfoyle and A.B. Baggeroer. The state of the art in underwater acoustic telemetry. *Oceanic Engineering, IEEE Journal of*, 25(1):4–27, Jan 2000.

[18] Peterson Roger L., Borth David E., and Ziemer Roger E. *An Introduction to Spread-Spectrum Communications*. Prentice-Hall, Inc., Upper Saddle River, NJ, USA, 1995.

[19] J.G. Proakis, E.M. Sozer, J.A. Rice, and M. Stojanovic. Shallow water acoustic networks. *Communications Magazine, IEEE*, 39(11):114–119, Nov 2001.

[20] John Proakis. *Digital Communications 3rd edition*. McGraw-Hill Science/Engineering/Math, 1995.

[21] R. E. Sheriff and L. P. Geldart. *Exploration Seismology*. Cambridge University Press, 2 edition, August 1995.

[22] E.M. Sozer, M. Stojanovic, and J.G. Proakis. Underwater acoustic networks. *Oceanic Engineering, IEEE Journal of*, 25(1):72–83, Jan 2000.

[23] M. Stojanovic. *Acoustic (underwater) Communications, Wiley Encyclopedia of Telecommunications*. John Wiley and Sons, jan 2003.

[24] Milica Stojanovic and Lee Freitag. Multichannel detection for wideband underwater acoustic cdma communications. *Oceanic Engineering, IEEE Journal of*, 31(3):685–695, July 2006.

List of Figures

Appendix A

Case	*Date*	*Time*	*Latitude*	*Longitude*
1	02. November 2005	19.00.27	63.5633°	7.0395°
2	31. March 2006	14.10.43	64.330°	6.8366°
3	18. April 1999	02.09.43	64.3315°	8.5188°
4	15. April 1997	04.37.00	64.199°	8.7813°

Table A.1: Detailed description of the sound speed profiles presented in figure 4.9.